Sensory Input Transformation in Layer 4 of Primary Somatosensory Cortex

Peng Gong

A dissertation submitted to the faculty of the University of North Carolina at Chapel Hill in partial fulfillment of the requirements for the degree of Doctor of Philosophy in the Department of Biomedical Engineering.

Chapel Hill
2008

Approved by,

Advisor: Associate Professor Oleg V. Favorov

Reader: Professor Henry S. Hsiao

Reader: Professor Douglas G. Kelly

Reader: Associate Professor Mark Tommerdahl

Reader: Professor Barry L. Whitsel

ABSTRACT

Peng Gong: Sensory Input Transformation in Layer 4 of Primary Somatosensory Cortex
(Under the direction of Dr. Oleg V. Favorov)

Neural representation of sensory information in the cerebral cortex undergoes a series of transformations, starting from its initial form at the level of thalamic neurons through a succession of cortical layers of multiple cortical areas. In the somatosensory system, the first such transformation takes place in the input layer, or Layer 4, of area 3b. This study explores several of its known properties: (1) the cortex is organized as a set of minicolumns, each a radial cord of cells 30-50 μm in diameter; (2) receptive fields of neighboring minicolumns occupy shuffled positions on the skin; (3) Layer 4 neurons possess more complex functional properties than the thalamic neurons from which they receive their inputs; and (4) neighboring neurons are decorrelated in their stimulus response behaviors. The neural mechanisms responsible for these properties were investigated in this study in a computational model of a field of minicolumns with self-organized Hebbian thalamocortical connections. A parametric study of this model optimized its performance on an “omnipotency” test, which measures the capacity of a set of Layer 4 neurons in the model to represent arbitrarily defined nonlinear functions. The maximal omnipotency was achieved in the model in which: (1) adjacent minicolumns had fixed inhibitory interconnections; (2) more widely separated minicolumns had

anti-Hebbian inhibitory interconnections; and (3) each neuron was modeled as an electric circuit consisting of two serially connected electrical compartments, with thalamic and anti-Hebbian inhibitory connections terminating in the distal compartment, and the fixed inhibitory connections terminating in the proximal compartment. When optimized for omnipotency, such a model exhibited among its emergent properties the shuffled receptive fields, decorrelated stimulus-response behaviors, and higher-order functional properties characteristic of the real cortical networks. In conclusion, this modeling study suggests that stimulus information is transformed in Layer 4 to maximize its linear coding of higher-order stimulus features via (1) fixed inhibitory interactions among adjacent minicolumns, carried out by connections of chandelier cells on the initial axon segments of spiny-stellate cells; and (2) anti-Hebbian inhibitory interactions among more distant minicolumns, carried out by connections of basket cells on the somata and dendrites of the spiny-stellate cells.

To my closest people in this world, my wife, Yixing Zhou,

who never gives up on me and always protects me, comforts me, encourages me and loves me.

To my parents, Hongbin Hu and Benzhi Gong,

who have always been indispensable throughout my life;

and who always love me and provide me a home and shelter.

To my parents in law, Fengzhen Zhang and Yuehan Zhou,

who always encourage me and believe in me,

support me and love me.

To my upcoming baby,

who brings me luck and happiness

in this fruitful 2008.

ACKNOWLEDGEMENTS

First of all, I would like to thank my dissertation advisor, Dr. Oleg V. Favorov. Without Dr. Favorov, I can hardly fulfill my PHD dream, as well as my parents' dreams. Dr. Favorov is a wonderful and patient mentor who has taught me so much, and has believed in me and encouraged me especially through these treasurable months.

Secondly, I would like to thank especially my academic advisor, Dr. Henry S. Hsiao. Without Dr. Hsiao, I can hardly fulfill my dream to be a UNC graduate, as well as my parents' dreams. Dr. Hsiao has inspired me in many ways during my years at UNC. I feel truly grateful to have him as my academic advisor.

Thirdly, I would like to thank Dr. Mark Tommerdahl, Dr. Barry L. Whitsel and Dr. Douglas G. Kelly to be kind enough to sit in my PHD committee, offer their sincere advice and share their valuable experience.

Finally, I would like to thank my family and friends for their unreserved support throughout my graduate study at UNC, especially Dr. Carol N. Lucas, Dr. Harvey A. Zar, and Dr. Benjamin M. W. Tsui.

TABLE OF CONTENTS

LIST OF TABLES

Table

LIST OF FIGURES

Figure

CHAPTER 1

INTRODUCTION

The cerebral cortex is the body organ whose task is, most fundamentally, to process sensory information. This information enters the cortex via the thalamus in its "raw" form, in which stimuli are reflected in the spatiotemporal patterns of activities of the thalamic cells in an essentially isomorphic (photographic image-like) and difficult to interpret manner. In the cortex this initial representation of the sensory information undergoes a series of transformations in a more-or-less hierarchical sequence of cortical areas, which extract and make progressively more explicit the neural representation of the behaviorally significant information (Bankman et al., 1990). The nature of these transformations and the neural mechanisms that accomplish them remain poorly understood. This dissertation investigates the first of these transformations in the somatosensory system, which takes place in the input layer, or ***layer 4***, of the cytoarchitectonically defined Brodmann's ***area 3b*** of the primary somatosensory cortex (SI). Area 3b receives input primarily from cutaneous mechanoreceptors and responds to tactile stimuli.

Information from skin receptors is transmitted to the Ventral Posterior Lateral (VPL) nucleus in the thalamus via synaptic relay in the Dorsal Column Nuclei (DCN) of the brainstem. From VPL this information is delivered to neurons comprising layer 4 of area 3b in SI, as well as to neurons in the other cortical areas that make up SI

(i.e., areas 3a, 1, and 2). The information that flows from the skin via the thalamic relay to the cortex is reflected in the receptive fields of somatosensory receptors and DCN, VPL and cortical neurons. Receptive field of a neuron is the sensory area within which a stimulus can evoke a response of the neuron. The receptive fields of somatosensory receptors are very small and uniformly excitatory. Since the receptive fields of the relay neurons are defined by the presynaptic afferent neurons that converge on them, their receptive fields grow in size. In addition, inhibitory interneurons participate and reshape the receptive fields of higher-level neurons to have both excitatory and inhibitory subregions, which enhance the contrast between stimuli. Although along the ascending somatosensory pathways each presynaptic neuron has divergent presynaptic connections with multiple postsynaptic neurons, and each postsynaptic neuron has convergent postsynaptic connections with multiple presynaptic neurons, the topographic arrangement of receptive fields is preserved (to varying degrees) in the thalamus and in the somatosensory cortex.

The excitatory and inhibitory regions of receptive fields can not only enhance the contrast between stimuli, but also give rise to more complex feature-detecting abilities of higher-order neurons. To illustrate on an example from the visual system, the receptive fields of retinal bipolar and ganglion cells and thalamic neurons in the lateral geniculate nucleus (LGN) are roughly circular and share an antagonistic center-surround organization. Their receptive fields are either ON-CENTER or OFF-CENTER and they respond optimally to differential illumination of the receptive field center and surround. The ON-CENTER cell can be most effectively excited by a small spot of light applied on the circular center of its receptive field and inhibited by

a ring of light shining on the entire surround of its receptive field. The responses of the OFF-CENTER cell are the opposite. Diffuse illumination on the entire receptive field of either the ON-CENTER or OFF-CENTER cell will produce only weak responses because the evoked excitation and inhibition cancel each other out almost completely. Therefore, due to their ON-CENTER or OFF-CENTER receptive fields, the bipolar cells, ganglion cells and neurons in the lateral geniculate nucleus are capable of measuring local contrast in light intensity. However, neurons in the primary visual cortex (V1) respond weakly to a beam of light but best to a bar of light with a specific axis of orientation. Their receptive fields are no longer circular but elongated, with the excitatory region in the middle flanked by the inhibitory regions on one or both sides, or vice versa. The resulting rectilinear receptive fields enable cells in the primary visual cortex to respond optimally to light stimuli with matching geometrical characteristics – in this case a line, bar or edge – and axis of orientation. Therefore the higher-order neurons in the primary visual cortex are capable to detect a novel kind of feature: an edge with a specific axis of orientation. These receptive fields result from the appropriate thalamocortical connection pattern: the excitatory regions in the receptive fields of layer 4 cells in the primary visual cortex largely overlap with the receptive fields of their input ON-CENTER thalamic neurons in the lateral geniculate nucleus, and the inhibitory regions in the cortical receptive fields coincide with the receptive fields of their OFF-CENTER thalamic neurons in the lateral geniculate nucleus (see, for example, Miller et al., 2001). In addition, the feed-forward inhibition from interneurons driven by the thalamus plays an important role in this orientation tuning of layer 4 neurons, along with the feed-forward excitation

directly from the thalamus. The feed-forward inhibition dominates the feed-forward excitation in most non-preferred orientations. Only within a very narrow range around the preferred orientation, the feed-forward excitation exceeds the feed-forward inhibition. The feed-forward inhibition thus helps to further sharpen the orientation tuning of layer 4 neurons.

The cerebral cortex is organized into vertical columns running through the entire six layers of the cerebral cortex from the pial cortical surface to the white matter (Mountcastle, 1978, 1997). This columnar organization is regarded as the basic structural principle of the cerebral cortex. This columnar organization is determined by intrinsic connectivity of the cerebral cortex, which is dominantly vertical. The spiny stellate neurons, located in the input layer 4, are the principal neurons receiving afferent input from the thalamus or other cortical areas. The pyramidal neurons are located in almost every layer, except for layer 1, and they are the principal output neurons. The axons of the spiny stellate neurons spread vertically towards the surface of the cerebral cortex. Also both the apical dendrites and axons of the pyramidal neurons are oriented perpendicular to the cortical surface, thus parallel to the axons of the spiny stellate neurons, and forming vertical bundles, which establish the anatomical basis of the vertical columns. Figure 1.1 illustrates the histology of the somatosensory cortex, and the vertical strands of cells are clearly identifiable there. The smallest possible unit of columnar organization is a single cell-wide column, termed a ***minicolumn***. The minicolumn is approximately 50 μm in diameter and 2 mm in depth, and composed of 80 to 100 cortical neurons. In 1978, Mountcastle proposed that the minicolumn is the smallest structural and

functional unit of the cerebral cortex, which has been since supported by extensive anatomical and physiological evidence (see for example a recent review by Tommerdahl et al., 2005).

Receptive fields of neurons located in close proximity to each other in the cortex are not uniform, but can vary prominently in their sizes, shapes, and positions on the skin. Figure 1.2, adapted from Favorov and Diamond (1990), illustrates such diversity in a typical near-radial microelectrode penetration of area 3b of a cat, in which 21 neurons were isolated and their receptive fields mapped. Significant differences in shape, size and skin position are evident in 21 individual receptive fields, though there is a very small common area shared by all the 21 individual receptive fields (see black region in the superimposed plot of the outlines of all 21 receptive fields in the left-bottom panel). Similarly diverse receptive fields among neighboring cortical neurons can be found in the primate somatosensory cortex (Powell and Mountcastle, 1959; McKenna et al., 1982; Iwamura et al., 1985; Favorov and Whitsel, 1988a,b; and Favorov and Diamond, 1990), in the visual cortex (Hubel and Wiesel, 1962, 1974a,b; Creutzfeldt et al., 1974; Albus, 1975a; Zohary et al., 1994; Gochin et al., 1991; Fujita et al., 1992; and Gawne and Richmond, 1993), and in the auditory cortex (Abeles and Goldstein, 1970).

Such diversity in receptive fields of neighboring cortical neurons is most prominent when those neurons are located in different minicolumns. Figure 1.3 schematically illustrates this idea on hypothetical data. On the left, shown as black dots are individual neurons in a Nissl-stained histological section of the primary somatosensory cortex. The physiological centers of receptive fields of these

neurons are shown as black dots in a two-finger figurine on the right. According to this figure, which summarizes experimental findings of Favorov and Whitsel (1988b), Favorov and Diamond (1990) and Tommerdahl et al. (1993), as long as neurons are located in the same minicolumn (e.g., neurons ***a-g*** in the figure), their receptive fields are very similar to each other. On the other hand, when neurons are compared across a sequence of minicolumns (e.g., neurons ***1-30***), their receptive fields bounce back and forth randomly around a common center, forming a cluster. Such seemingly random shuffling of receptive field centers is a characteristic of local groups of minicolumns, which are separated by sharp boundaries, crossing which shifts receptive fields to a new skin region. These sharp boundaries partition the somatosensory cortex into a honeycomb-like mosaic, resulting in larger columnar units named "***segregates***" (Favorov et al., 1987; Favorov and Whitsel, 1988a; Favorov and Diamond, 1990). A segregate is approximately 0.3-0.6 mm in diameter and consists of 60-80 minicolumns. The receptive fields of the minicolumns within a segregate together cover an extended skin region, although receptive fields of most minicolumns in a segregate overlap only minimally and, consequently, all together they share only a very small skin region in common, called the ***segregate receptive field center*** (see Figure 1.2). Segregate receptive field centers are arranged somatotopically across area 3b in an orderly two-dimensional map of the skin surface.

Columnar structures similar to segregates have been recognized in other sensory systems. For example, in the primary visual cortex, Hubel and Wiesel (1974a) described the "hypercolumn" which is composed of a group of minicolumns

responsive to light bar stimuli of all orientations from a particular region in the visual field. In rodent primary somatosensory cortex, Woolsey and Van der Loos (1970) discovered the “barrels” which are discrete structural and functional units that receive and process input from individual “principal” facial whiskers. In general, such larger-scale discrete vertical columnar units are called ***macrocolumns*** (Mountcastle, 1978). A macrocolumn is composed of minicolumns that share certain functional properties. Macrocolumns are regarded as computational modules, each of which receives specific input information, transforms that information, and sends the output to other higher-level associative cortical areas. The anatomical basis of macrocolumns is that minicolumns within the same macrocolumn share similar thalamocortical afferent input connections.

Traditionally, since the macrocolumn has been regarded as a functional module, the similarities among minicolumns within a macrocolumn have been emphasized. However, as reviewed above, there exist prominent differences in some of the functional properties among minicolumns within a macrocolumn, such as for example diversity in exact receptive field positions on the skin. In order to investigate the possible underlying mechanisms responsible for such diversity of receptive fields of minicolumns within a macrocolumn and their potential significance for the functional properties of the macrocolumn, Favorov and Kelly (1994a,b) developed a computational model of a single macrocolumn as a set of 61 minicolumns.

The model’s connectional architecture is shown in Figure 1.4. In it the thalamic nucleus receives input from the two-dimensional “skin” and then relays it to

the cortex. The receptive fields of the thalamic neurons are circular and are topographically arranged on the skin, thus resulting in a two-dimensional array on a two-dimensional surface. The cortex in this computational model is composed of regular hexagon-shaped macrocolumns, each macrocolumn is made up of 61 cylinder-shaped minicolumns, and each minicolumn is represented by three cortical cells of three distinct types: a ***spiny stellate*** cell, a ***pyramidal*** cell and a ***double bouquet*** cell. The spiny stellate cell receives excitatory afferent input from multiple thalamic neurons and feed-forwards the excitation to the pyramidal cell and the double bouquet cell within the same minicolumn, and to a smaller magnitude, to the neighboring spiny stellate cells up to two minicolumns away. The double bouquet cell inhibits only the pyramidal and spiny stellate cells of the immediately adjacent minicolumns. The synaptic connections between the thalamic neurons and the spiny stellate cells are plastic. The thalamocortical synaptic connection strengths are initialized randomly and then adjusted according to the Hebbian Synaptic Plasticity Rule until they are stabilized during the “developmental” stage in which the whole thalamocortical network is trained by a long series of point stimuli on the two-dimensional skin surface. All the other synaptic connection strengths are predetermined and fixed throughout the simulation. In the following text, this computational model will be referred to as the ***1994 Favorov-Kelly model***.

The 1994 Favorov-Kelly model successfully reproduced experimental observations of shuffled receptive fields of minicolumns within the same macrocolumn. However, it has two noteworthy limitations. The first limitation is that there are still somewhat significant discrepancies between real cortical neurons and

simulated neurons based on the 1994 Favorov-Kelly model in functional properties, such as orientation tuning. The model cells can develop only very modest orientation tuning, much weaker than that of real neurons in the primary somatosensory cortex (Bensmaia et al., 2008).

The second limitation concerns the double bouquet cell, which is proposed to provide fixed lateral inhibition in the 1994 Favorov-Kelly model. There are two problems associated with the double bouquet cell. The first problem is that only in primates double bouquet cells contact spiny-stellates (Casanova, 2005), which renders the 1994 Favorov-Kelly model more specialized and less generic. The second problem is that even in primates double bouquet cells cannot exert strong enough inhibition on spiny stellate cells. The closer the inhibition is to the axonal output part of a neuron, the more effective the inhibition is. Real double bouquet cells synapse on dendrites of spiny stellate cells, which correspond to the distal electrical compartment of the spiny stellate cells in the 1994 Favorov-Kelly model. However, in the 1994 Favorov-Kelly model, fixed lateral inhibition is placed in the proximal electrical compartment, which corresponds to the soma of spiny stellate cells. Therefore, the double bouquet cell is not a good candidate for providing fixed lateral inhibition in the 1994 Favorov-Kelly model.

In this dissertation work, we developed a computational system largely based on the 1994 Favorov-Kelly model to simulate information processing in cortical layer 4 of a macrocolumn composed of minicolumns. Besides addressing the above two limitations, we used this system to investigate the potential contribution of lateral inhibition to two other important properties of sensory input transformation in layer 4.

The first property is that the activities of neighboring cortical neurons are essentially fully decorrelated. It is well known that neurons located in close proximity to each other in cortical gray matter tend to have similar stimulus response properties, and thus they tend to respond similarly to test stimuli. They are also known to synchronize their spike discharges temporarily in response to some of the test stimuli. However, despite such notable similarities, the response properties of nearby cortical neurons are still quite diverse (as reviewed above), so that across the full repertoire of stimulus patterns experienced in the individual's regular life, neighboring cortical neurons turn out to be essentially fully **decorrelated** in their response behaviors. That is, when compared across ethologically representative sets of stimuli, responses of neighboring neurons in a cortical column are found close to be statistically independent (Gawne and Richmond, 1993; Ghose et al., 1994; Zohary et al., 1994; Gawne et al., 1996; Vinje and Gallant, 2000; Reich et al., 2001).

The second property that we postulate for the layer 4 transform of its afferent information might be defined as a "***hidden information maximization***" principle. To explain, considering information coding abstractly, the same information can be coded, or represented, in a set of information-carrying channels in a wide variety of ways. The coding strategies can vary, however, in how computationally easily can this information be "read" by an intended "user" (or, in other words, be isolated or extracted or, in general, made use of in interpretation or decision making). The **algorithmic complexity of information extraction/utilization** can vary from the simplest (using a dedicated channel to represent this and only this information) to

very complex (requiring highly nonlinear integration of the states of many channels). The dedicated channel strategy is not practical because of its limited representational capacity, compared to ***distributed*** codes, in which multiple channels carry information about a given item together with information about some other such items.

Among the distributed codes, the algorithmically simplest ones are those that to extract particular information require only linear summation of the states of the relevant channels. Such codes can be easily used by biological neurons, by linear dendritic summation of their synaptic inputs. We can call this linear-summation type of information representation "***explicit***." In contrast, the codes that require algorithmically complex (nonlinear) means of information extraction can be called "***implicit***."

Using this terminology, we can state that most of the information coming from the outside world to the brain is represented only implicitly by the activities of sensory receptors. Such "deeply hidden," or "high-level," information is also turns out to be most important to situation comprehension and behavioral decision making. The basic task of the sensory cortex is to convert the originally implicit representations of behaviorally-significant information into algorithmically simpler – explicit – representations suitable for behavioral decision making. This task is accomplished by the cortex incrementally and requires participation of multiple cortical areas.

Considered in this light, the task of layer 4 input transform might be expected to be to make explicit in its output as much of hidden, or implicit, behaviorally-

significant sensory information as possible. However, layer 4 of the primary somatosensory cortex, as the first stage in sensory input transformation, might not be in a position to anticipate which information items might be behaviorally significant and therefore should be made more explicit. Instead, a more general "***omnipotency***" strategy might be to **make more explicit as much of the hidden sensory information as possible**. Such an omnipotency strategy, referred to as ***kernel-based methods***, has been found highly successful in computational fields of Machine Learning and Pattern Recognition (Vapnik, 1995; Schölkopf and Smola, 2002).

In developing our minicolumnar model of somatosensory cortical layer 4 network, we hypothesized that in order to achieve maximal omnipotence, the neurons in layer 4 must be essentially decorrelated, which would require strong lateral inhibition among them. In turn, lateral inhibition can bring about nonlinearity in information transformation in cortical layer 4, which is necessary for extracting hidden information. In the following chapters, we show that omnipotency, decorrelation, inhibition, and receptive field shuffling do indeed go together and their optimization endows the model network with biologically realistic properties.

Figure 1.1. Histological section of primate somatosensory cortex.
Radial strands of cells, or minicolumns, are clearly visible in this Nissl-stained section.

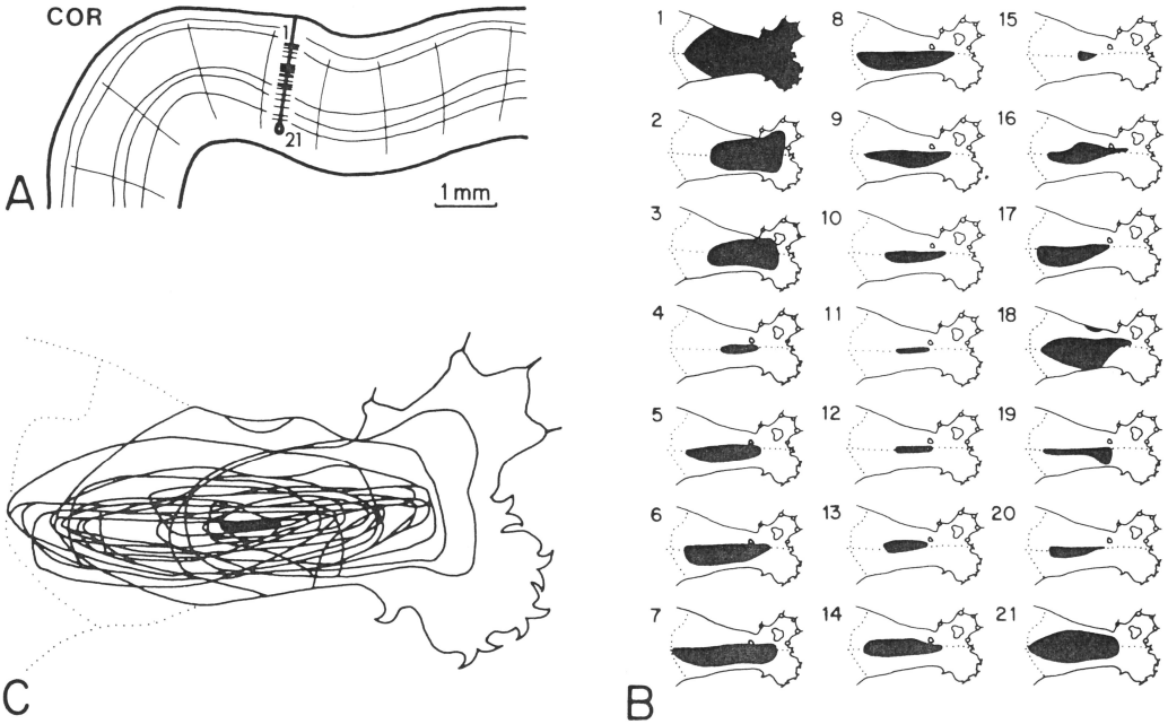

Figure 1.2. Local receptive field diversity in primary somatosensory cortex.
A, 21 single units were isolated in this typical near-radial microelectrode penetration of cat's primary somatosensory cortex. Their receptive fields are shown in B, and plotted superimposed in C. COR - coronal sulcus. The blackened region in C is included in all 21 receptive fields (from Favorov and Diamond, 1990).

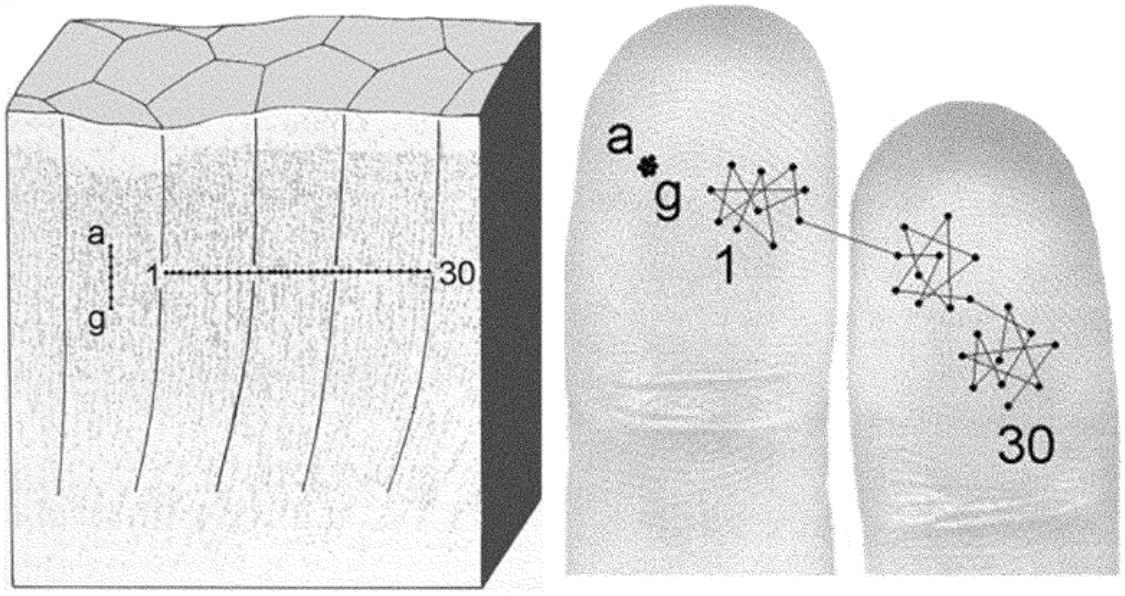

Figure 1.3. A hypothetical illustration of shuffled minicolumnar receptive field centers and macrocolumnar organization.
Hypothetically, in the somatosensory cortical area receiving input from fingers, a series of neurons a-g, confined within a single minicolumn have very close receptive field centers. A series of neurons 1-30, located in a series of minicolumns, have receptive field centers that do not shift continuously but bounce back and forth forming several clusters with sharp boundaries. Those boundaries partition the cortex into honeycomb-like mosaic, termed "segregates" in the somatosensory cortex, or "macrocolumns" in general (from Tommerdahl et al., 2005).

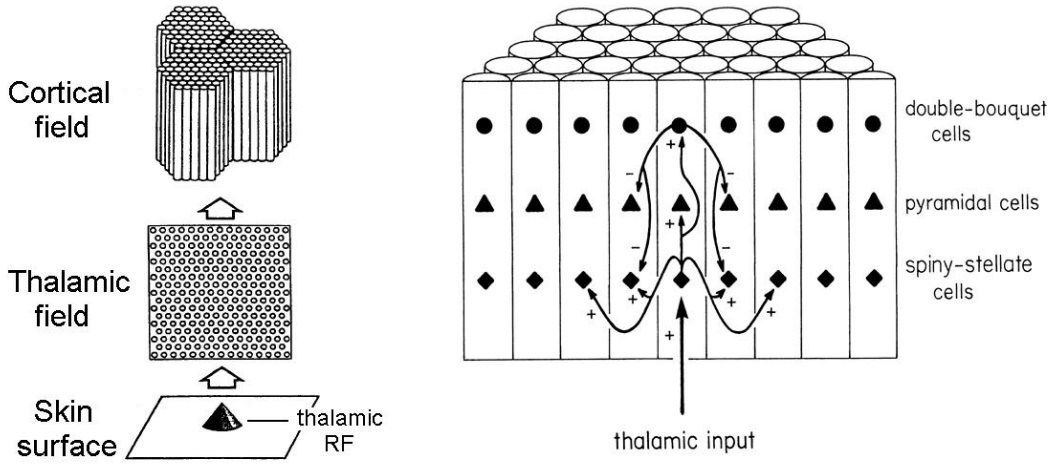

Figure 1.4. 1994 Favorov-Kelly model.
The basic scheme of the 1994 Favorov-Kelly model and its settings for synaptic connections are illustrated. On the left, somatosensory information processing is simplified to consist of only three layers: the skin layer, the thalamic layer and the cortical layer. Thalamic units have circular receptive fields with identical size in the skin field. The mapping from the skin field to the thalamic field is perfectly somatotopic. Stimuli delivered within the skin field are transmitted to thalamic units first and in turn relayed to cortical units. The cerebral cortex is modeled to be organized into regular hexagon-shaped macrocolumns and a macrocolumn is modeled to be composed of 61 cylinder shaped minicolumns. On the right, a minicolumn is modeled to consist of three representative cells: input spiny-stellate cells (denoted by solid diamonds), output pyramidal cells (denoted by solid triangles), and inhibitory double-bouquet cells (denoted by solid circles). The spiny-stellate cell receives excitatory thalamic input and relays it to the pyramidal cell and the double-bouquet cell within the same minicolumn. To a less extent, the spiny-stellate cell also excites the spiny-stellate cells in its neighboring minicolumns within a radius of two minicolumns. The double-bouquet cell inhibits the pyramidal cells and the spiny-stellate cells in its immediate neighboring minicolumns within a radius of one minicolumn (from Favorov and Kelly, 1994a).

CHAPTER 2

METHODS

Our current computational system was developed primarily based on the 1994 Favorov-Kelly model (Favorov and Kelly, 1994a,b). The three-layer hierarchical organization of the 1994 Favorov-Kelly model (Figure 2.1) was retained. It includes a skin layer, a layer of thalamic units representing thalamic neurons, and a layer of minicolumnar units representing layer 4 part of minicolumns. The skin is modeled as a two-dimensional flat surface. The receptive fields of the thalamic units are topographically arranged on the skin and have identical circular shape and identical size. During computer simulations, multi-point stimuli are applied to the skin field. The activity of each thalamic unit evoked by a single point stimulus is solely determined by the distance between the position of the point stimulus and the receptive field center of the thalamic unit in the skin field. The activity of each thalamic unit evoked by a multi-point stimulus is calculated as the sum of the activities of that thalamic unit evoked by each component point stimulus individually. A minicolumnar unit receives excitatory afferent inputs from all the thalamic units. Inputs from thalamic units and lateral inputs from surrounding minicolumnar units are the driving forces to shape the receptive fields and functional properties of minicolumnar units. The thalamocortical synaptic connections are plastic. The lateral connections are inhibitory.

As in 1994 Favorov-Kelly model, a single macrocolumn is modeled as composed of 61 minicolumnar units organized into a regular hexagon shape structure (Figure 2.1). Each minicolumn is represented by a prototypical neuron that is modeled as a two-compartmental electrical circuit (illustrated in Figure 2.2). Each minicolumn inhibits its immediate neighboring minicolumns via fixed inhibitory lateral connections and it also inhibits all other 60 minicolumns via Anti-Hebbian plastic inhibitory lateral connections.

Both the excitatory thalamocortical afferent connections and the Anti-Hebbian plastic inhibitory lateral connections are modifiable according to the Hebbian Rule (Fyffe, 2005) in the “connection development” stage of computer simulations. The correlation between the activity of a thalamic unit and the activity of a minicolumnar unit is used to determine the strength of Hebbian excitatory thalamocortical connection between them. The correlation between activities of two minicolumns is used to determine the strength of the Anti-Hebbian plastic inhibitory lateral connection between them. The strength of the fixed lateral inhibitory connections between immediate neighboring minicolumns is constant and uniform.

In this newly developed computational system, the minicolumn-representing neuron is modeled as a two-compartmental electrical circuit, illustrated in Figure 2.2. The two compartments are differentiated as the distal compartment and the proximal compartment. In the 1994 Favorov-Kelly model, the spiny stellate cell was modeled as a two-compartmental electrical circuit with the distal compartment referred to the distal dendrites and the proximal compartment referred to the proximal dendrites and soma. The fixed lateral excitatory inputs and the fixed lateral inhibitory inputs were

placed on the distal compartment and the proximal compartment, respectively. In our new system lateral excitation is excluded and two types of lateral inhibition are placed on the distal compartment and the proximal compartment. In Figure 2.2, G_{de} is the conductance of excitatory synapses on the distal compartment. G_{di} and G_{pi} are the conductances of inhibitory synapses on the distal compartment and the proximal compartment, respectively. G_{dm} and G_{pm} are passive membrane conductances of the distal compartment and the proximal compartment, respectively. G_L is the longitudinal conductance connecting the distal compartment and the proximal compartment. E_{de} is the reversal potential of excitatory synapses on the distal compartment. E_{di} and E_{pi} are the reversal potentials of inhibitory synapses on the distal compartment and the proximal compartment, respectively. E_{dr} and E_{pr} are resting membrane potentials of the distal compartment and the proximal compartment, respectively. V_d and V_p are membrane potentials of the distal compartment and the proximal compartment, respectively.

Computer simulation of the model is divided into two stages. The first stage is the “connection development” or “self-organization” stage. Initially, the weights of thalamocortical connections and the Anti-Hebbian plastic inhibitory lateral connections are assigned randomly. Then the system is trained by applying randomly picked multi-point stimuli to the skin. The reason that we chose to use multi-point stimuli instead of single-point stimuli was to increase the complexity of training patterns in order to explore the state space more extensively. The second stage is the “evaluation” stage during which we ran various tests on the developed

system.

The connection-development program updated the plastic connections after every 1000 randomly generated 5-point stimuli. In response to each five-point stimulus applied to the skin field, we calculated the instantaneous firing rate for each minicolumn-representing neuron. First, we calculated the activity of every thalamic unit evoked by each of the five points. The activity F_{ij}^{TH} of the thalamic unit i evoked by the single-point stimulus j was calculated as:

$$F_{ij}^{TH} = F_{\max}^{TH}(1-\frac{D_{ij}}{R^{TH}})^{+},$$

where $F_{\max}^{TH}$ = 1 is the maximal possible activity of a thalamic unit which could be evoked by a single-point stimulus. D_{ij} is the distance from the position of the point stimulus j to the receptive field center of the thalamic unit i. R^{TH} is the radius of the receptive field of a thalamic units and it was set to 3, as in 1994 Favorov and Kelly model. The plus sign indicates the calculated value inside the parentheses should be set to zero if it is negative. Next, the activity F_i^{TH} of the thalamic unit i evoked by the five-point stimulus was calculated as the sum of activities of the thalamic unit i evoked by each of the five points individually:

$$F_i^{TH} = \sum_{j=1}^{5} F_{ij}^{TH}$$

The force f of every five-point stimulus applied on the skin gradually increased from zero magnitude to full magnitude (set to 1) in 10 time steps and was held for the next 40 time steps, as illustrated in Figure 2.3. For each time step, the total thalamic input F_i^{AF} to minicolumn neuron i was then calculated as:

$$F_i^{AF} = f\sum_{j=1}^{127}(W_{ij}^{TH} F_j^{TH}),$$

where W_{ij}^{TH} is the strength of the thalamocortical synaptic connection between the thalamic unit j and neuron i. Next, the conductances of the excitatory and inhibitory synapses on the distal compartment and the inhibitory synapses on the proximal compartment were calculated according to the following differential equations:

$$\mu\frac{d}{dt}G_i^{de} = -G_i^{de} + F_i^{AF}$$
$$\mu\frac{d}{dt}G_i^{di} = -G_i^{di} + C^{di}\sum_j W_{ij}^{di} F_j^{MC}$$
$$\mu\frac{d}{dt}G_i^{pi} = -G_i^{pi} + C^{pi}\sum_k F_k^{MC}$$

where F_j^{MC} is the output activity of minicolumn *j*, μ is a time constant, C^{di} and C^{pi} are scaling constants for inhibition in the distal and proximal compartments, respectively, and W_{ij}^{di} is the weight of the inhibitory connection from minicolumn *j* to minicolumn *i*. These differential equations were solved numerically using Euler method as follows:

$$G_i^{de}(t+\Delta t) = (1-\Delta t/\mu)G_i^{de}(t) + (\Delta t/\mu)F_i^{AF}(t)$$
$$G_i^{di}(t+\Delta t) = (1-\Delta t/\mu)G_i^{di}(t) + (\Delta t/\mu)C^{di}\sum_j W_{ij}^{di} F_j^{MC}(t)$$
$$G_i^{pi}(t+\Delta t) = (1-\Delta t/\mu)G_i^{pi}(t) + (\Delta t/\mu)C^{pi}\sum_k F_k^{MC}(t)$$

The time step Δt and time constant μ were set to 1 millisecond and 4 milliseconds, respectively. $\sum_k F_k^{MC}$ denotes the summation of activities of immediately neighboring minicolumns. $\sum_j W_{ij}^{di} F_j^{MC}$ denotes the weighted summation of activities of all other 60

minicolumns. The membrane potential V^d of the distal compartment and the membrane potential V^p of the proximal compartment are determined as follows:

$$V^d = \frac{G^{de}(G^{pi} + G^L + 1)}{(G^{de} + G^{di} + 1)(G^{pi} + G^L + 1) + G^L(G^{pi} + 1)}$$

$$V^p = \frac{G^{de}G^L}{(G^{de} + G^{di} + 1)(G^{pi} + G^L + 1) + G^L(G^{pi} + 1)}$$

where G^L is the longitudinal conductance connecting the distal compartment and the proximal compartment. The "activity," in a form of an instantaneous firing rate, F_i^{MC} of the neuron representing minicolumn i is determined by its membrane potential of the proximal compartment V^p:

$$F_i^{MC} = \frac{(V^p)^3}{0.01 + (V^p)^3}$$

At the end of each round of 1000 randomly chosen five-point stimuli, the plastic connections were updated as follows:

$$W_{ij}^{TH} = [(1 - RM) \cdot W_{ij}^{TH} + RM \cdot sign(corr(V_i^d, F_j^{TH})) \cdot (corr(V_i^d, F_j^{TH}))^2]^+$$

$$W_{ij}^{di} = [(1 - RM) \cdot W_{ij}^{di} + RM \cdot corr(V_i^d, F_j^{MC})]^+$$

RM is the rate of connection maturation, set to 0.1. $sign()$ function outputs positive or negative sign depending on the value inside the parenthesis. $corr()$ function calculates the correlation between given variables. Therefore, the synaptic strength of the thalamocortical connection between a minicolumnar unit and a thalamic unit was determined by the correlation between the distal membrane potential of the minicolumnar unit and the activity of the thalamic unit; while the synaptic strength of the Anti-Hebbian plastic lateral inhibitory connection between a presynaptic minicolumnar unit and a postsynaptic minicolumnar unit was determined

by the correlation between the output activity of the presynaptic minicolumnar unit and the distal membrane potential of the postsynaptic minicolumnar unit. These correlations were computed over the values of the variables taken on the 50th time step of the network's responses to 1000 randomly chosen 5-point skin stimuli. In order to prevent the activities of minicolumns from becoming excessively large or invariably zero, we normalized the thalamocortical connection weights of each neuron by summing all of its thalamocortical connection weights and then dividing each thalamocortical connection weights by this sum. Finally, to ensure that all neurons will have the average output activity in response to 5-point stimuli close to a certain desired value (chosen to be 0.075), the normalized thalamocortical connection weights were further scaled by $0.075/\overline{FSS_i}$, where $\overline{FSS_i}$ is the average activity of neuron i across the previous 1000 stimuli.

After the excitatory thalamocortical afferent connections and the Anti-Hebbian plastic inhibitory lateral connections were fully developed, we characterized the system's performance by computing the average distance between receptive field centers of immediate neighboring minicolumns and the average correlation between activities of all pairs of minicolumns in response to 1000 randomly chosen 5-point stimuli. We then ran an omnipotency test.

As the system was developing its plastic connections, the trajectories of the receptive field centers were displayed in real time to monitor the progress of the connection development. When the system reached the steady state, the receptive field centers stopped traveling. Then we generated a "receptive field shuffling" plot by connecting the receptive field centers of immediate neighboring minicolumns with

straight lines to demonstrate their relative positions and how well they shuffled. The less the lines crossed one other, the less prominently the receptive field centers of minicolumns within the same macrocolumn shuffled. The average distance between receptive field centers of adjacent minicolumns was calculated to indicate to what extent the receptive field centers of immediate neighboring minicolumns were separated. The greater the average distance was, the more spread out the receptive field centers were and the more they shuffled. We also produced a color-coded map to demonstrate the positions of receptive field centers of the minicolumns on the skin. Different colors were used to distinguish different regions of the skin field. The receptive field centers were represented by white dots scattered in the color-coded skin field. In the accompanying color-coded honeycomb-like macrocolumn image, each of the 61 minicolumns was colored depending on the color of the region in the skin field where its receptive field center was located. A pattern of gradual transition or systematic alternation in color of 61 minicolumns within the same macrocolumn would indicate a somatotopic map. We expect to observe each minicolumn in a distinctive color and the colors of neighboring minicolumns referred to very different regions of the skin field.

In order to assess how well the 61 minicolumns within the same macrocolumn were decorrelated, we calculated the correlations between the activities of every pair of minicolumns, altogether 1830 pairs. Besides the average squared correlation, which could be used as an indicator of decorrelation, we generated the histogram of the correlations to further demonstrate and analyze the distribution of the correlations. Ideally, we would expect that the average correlation was nearly zero

and the histogram of the correlations demonstrated that the percentages of high correlations were nearly 0 and most correlations were negative or close to 0.

The network with fully developed thalamocortical and anti-Hebbian inhibitory connections was evaluated for its "omnipotency," defined as the capacity to represent any arbitrarily defined nonlinear features of stimulus patterns. Any such stimulus feature can be defined as a function over the stimulus/input space. Thus, our omnipotency test involves defining an arbitrary test function ***T(S)*** on an arbitrarily chosen set of 5-point stimuli $S_1 \ldots S_n$. Typically in our studies we use $n = 20$. The test function ***T(S)*** is given a value of 0 or 1 on each of the n test stimuli, such that for **each** thalamic unit the correlation coefficient between its responses to these n test stimuli and ***T(S)*** is equal to zero. This means that this test function – or stimulus feature – is "hidden" at the level of the thalamic units; i.e., it is represented only implicitly in the thalamic layer and cannot be extracted (i.e., made explicit) by any linear summation of the activities of the thalamic units.

Next, we compute the responses $F_1^{MC} \ldots F_{61}^{MC}$ of all 61 minicolumns to each of the n test stimuli. As a rule, because the minicolumnar output is a nonlinear transform of the thalamic input, the correlation coefficient between responses of any given minicolumn to the test stimuli and ***T(S)*** is most likely to be non-zero. The question is: Will the test function ***T(S)*** be represented explicitly – and to what degree – by outputs of the 61 minicolumns? How well would a hypothetical neuron in the other cortical layers be able to represent function ***T(S)*** by computing a weighted sum of outputs of the 61 minicolumns? Of course, if we used error-correction learning, we would be able to train such a neuron to produce 100% accurate outputs to the n

test stimuli (since the number of its input channels, 61, is much larger than the number of training samples, n = 20). However, assuming that cortical neurons do not use error-correction learning, but Hebbian learning, our hypothetical neuron will not be as successful. To approximate Hebbian limitations, for each minicolumn i we compute the correlation coefficient $r_{T,i}$ between $T(\mathbf{S})$ and the responses of that minicolumn to the n test stimuli. Now we can compute the output of the hypothetical neuron in response to a given test stimulus s as:

$$F(s) = \sum_{i=1}^{61} r_{T,i} \cdot F_i^{MC}(s).$$

How well will $F(\mathbf{S})$ approximate $T(\mathbf{S})$ on test stimuli $S_1 \ldots S_n$? We measure it by computing the correlation coefficient $r_{T,F}$ between $F(\mathbf{S})$ and $T(\mathbf{S})$, giving us the upper bound for the ability of the outputs of the 61 minicolumns together to linearly represent the test function $T(\mathbf{S})$.

Finally, to obtain a general estimate of this ability to represent arbitrary test functions, we repeat this test study 100 times, each time using different test functions $T(\mathbf{S})$ defined on different sets of test stimuli $S_1 \ldots S_n$, and use the average squared correlation coefficient $r_{T,F}^2$ as our **measure of representational omnipotency** of the studied minicolumnar network.

Lastly, to evaluate minicolumns for their sensitivity to orientation of elongated skin stimuli, for each minicolumn we applied a series of line stimuli centered on its receptive field center with varying orientations ranging from 0 degree to 179 degrees, in 1 degree steps. The line stimulus was simulated by exactly the same way as the multi-point stimuli used in connection development, except that in the latter case points were picked randomly while in the former case points were arranged in a

straight line. The activities of minicolumns evoked by those line stimuli in every orientation were recorded and displayed in two different ways. One was to simply plot the activity as a function of stimulus orientation. The other was to draw every line stimulus in its proper orientation, but with its length determined by the activity of the minicolumn in response to that line.

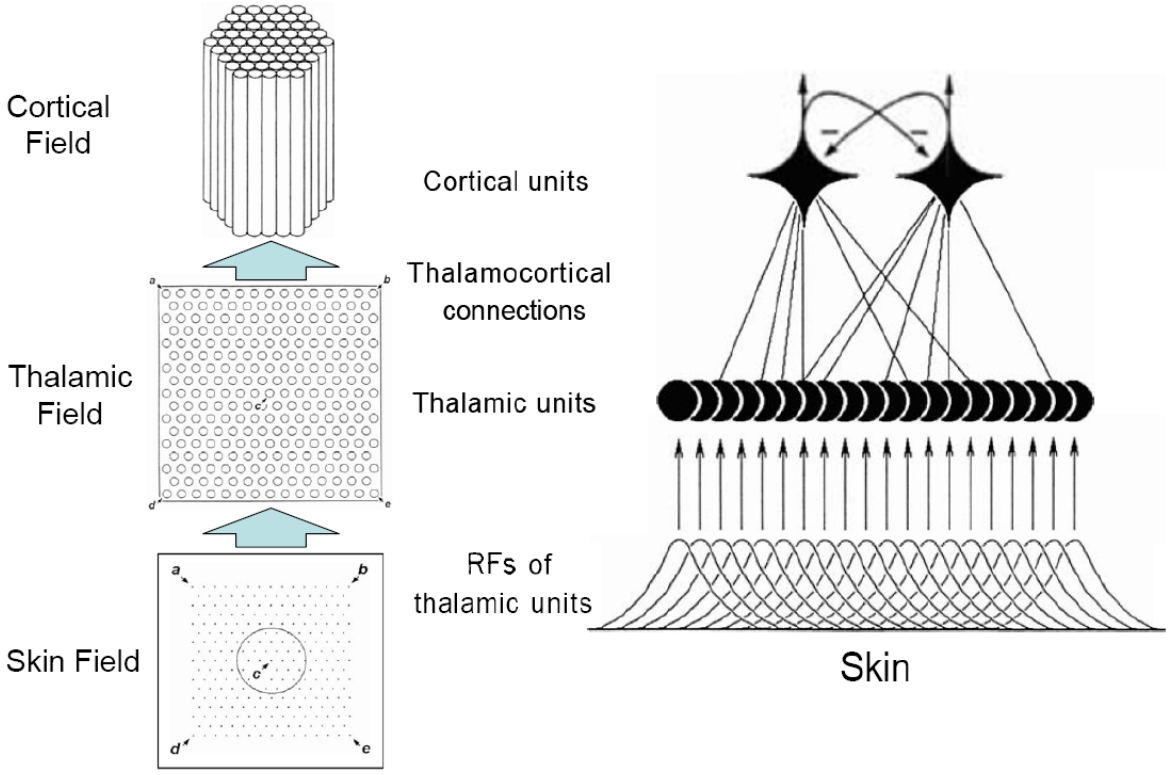

Figure 2.1. Three-layer structure of somatosensory minicolumnar model.
The functional module of cerebral cortex is assumed to be macrocolumn, which is composed of 61 minicolumns. Minicolumns, or cortical units, receive inputs from 127 thalamic cells. Thalamic cells receive inputs from the skin field. Each thalamic unit has a circular receptive field placed somatotopically on the skin.

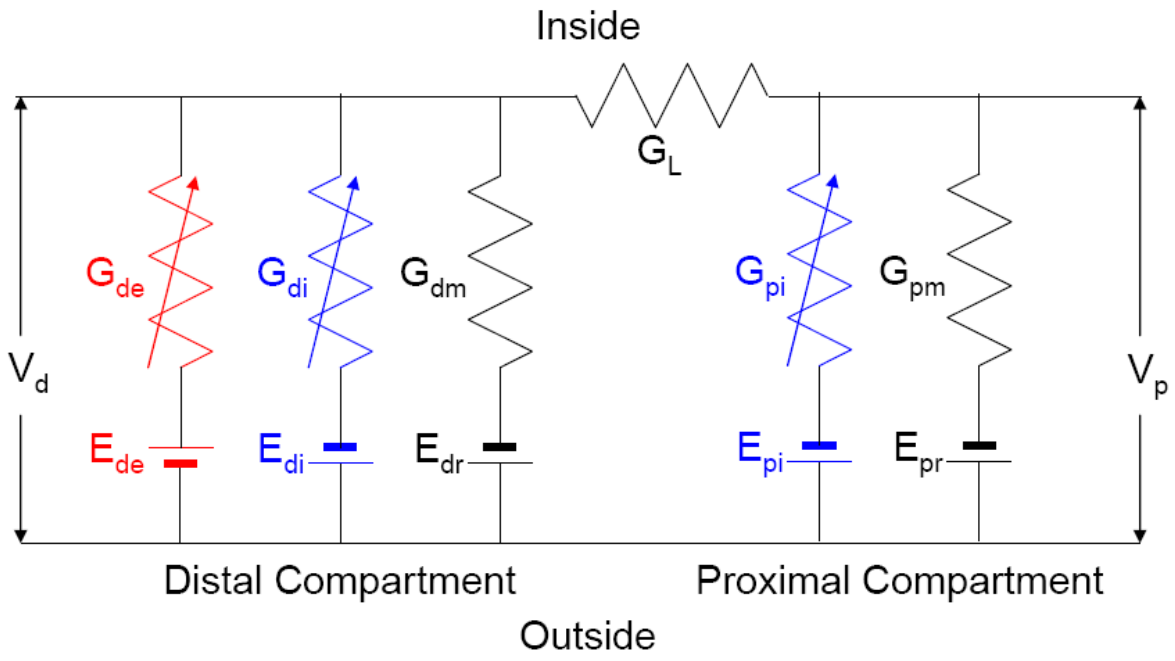

Figure 2.2. Neuron representing a minicolumn is modeled as a two-compartmental electrical circuit.

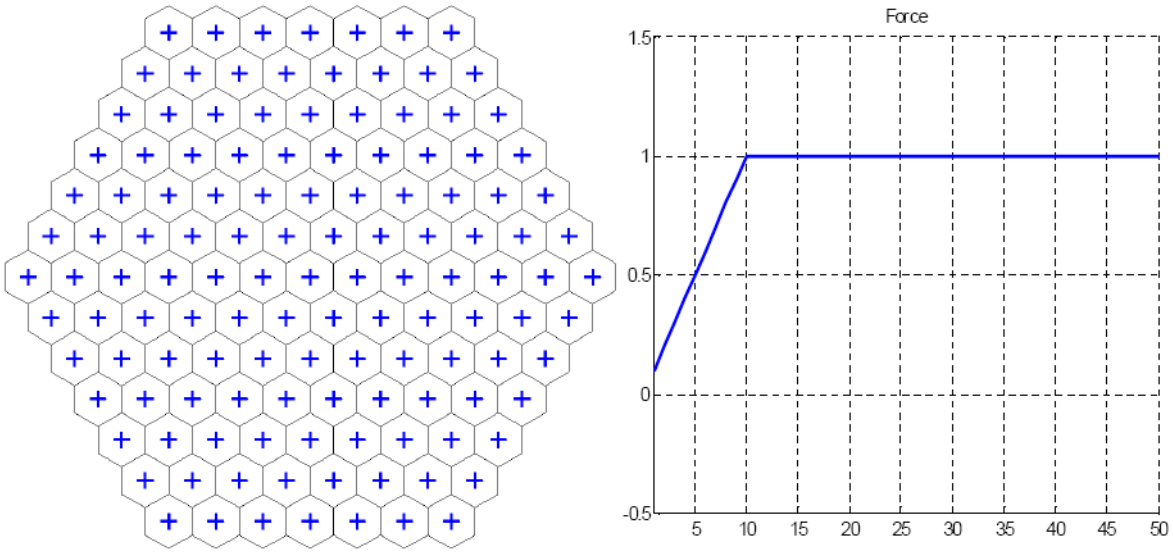

Figure 2.3. Coordinates of receptive field centers of thalamic units and stimulus strength as a function of time.
The left panel shows the coordinates of receptive field centers (blue crosses) of 127 thalamic units (white regular shaped hexagons). The right panel shows that stimulus strength increases from 0 to 1 in the first 10 time steps and remains at 1 for the next 40 time steps.

CHAPTER 3

RESULTS

We first establish that the new model can successfully reproduce the shuffled receptive fields of minicolumns similar to those obtained by the 1994 Favorov-Kelly model. As illustrated in Figure 3.1 – 3.6, the new model was not only able to reproduce the shuffled receptive fields of minicolumns, but also improved decorrelation among minicolumns.

The network's starting state before the development of thalamocortical connections and its stable state after the development are shown in Figures 3.1 – 3.6. Since there were significant modifications made to the 1994 Favorov-Kelly model, we used equivalent rather than identical parameters in our simulation to approximate the old results. All the parameters are documented in Tables 3.1 – 3.4, if not mentioned otherwise. Since the thalamocortical connections were prescribed randomly initially, the receptive field centers of 61 minicolumns within the same macrocolumn are randomly dispersed within a relatively small skin region with an average distance of 1.628 units between immediate neighboring minicolumns (Figure 3.1 – 3.2). In the circular color-coded skin map (Figure 3.2), most of the receptive field centers are scattered more towards the center of the skin. In the corresponding honeycomb shaped macrocolumn, there was no systematic alternation in color coding of 61 minicolumns (Figure 3.2). However, after the

thalamocortical connections reached the steady state, the receptive field centers of the 61 minicolumns within the macrocolumn become distributed in a much larger region with an average distance of 4.269 units between immediate neighboring minicolumns (Figure 3.4). Figure 3.4 demonstrates the relative positions of receptive field centers with lines connecting the immediate neighboring minicolumns. It was observed, interestingly, that the image is composed of numerous triangles rotating from and superimposed on each other. The circular color-coded skin map clearly demonstrates that the receptive field centers are scattered more towards the skin margins, resulting in a vast empty space at the center of the skin field (Figure 3.5).

Although the new model did successfully reproduce the shuffled receptive fields of the 61 minicolumns, the patterns of the shuffled receptive field centers were different between the new model and the 1994 Favorov-Kelly model (Favorov and Kelly, 1994 a). It was not only due to the non-identical parameters but also, more importantly, due to the modifications made to the 1994 Favorov-Kelly model. In short, the new model does not have parasynaptic influences from surrounding macrocolumns imposed on the 61 minicolumns within the central macrocolumn because only the central macrocolumn is modeled now. In the 1994 Favorov-Kelly model, the receptive field centers of the 61 minicolumns within the central macrocolumn reached the equilibrium when influences from the central macrocolumn were balanced with those from the surrounding 6 macrocolumns. Minicolumns that were closer to the borders of the central macrocolumn were more affected by the neighboring macrocolumns. Therefore, the 1994 Favorov-Kelly model produced a pattern in which the shuffled receptive field centers were more or

less distributed evenly throughout the skin field. However, in this new model, there are no such surrounding macrocolumns and parasynaptic influences. It is the strong fixed lateral inhibition between immediate neighboring minicolumns that is primarily responsible for driving the receptive field centers of all 61 minicolumns away from the center of the skin field. Because of the repulsive nature of the inhibition, the strong fixed lateral inhibition between immediate neighboring minicolumns tends to drive the receptive fields of minicolumns as far apart as possible. The above explanation is confirmed by the pattern of color alternation of the 61 minicolumns in the left panel of Figure 3.5. For example, the minicolumn at the upper rightmost corner of the macrocolumn is color-coded in vivid-blue, but two of its three immediate neighboring minicolumns are in brown and the third one is in green. From the corresponding color-coded skin field, the vivid blue is almost opposite to the brown and nearly opposite to the green.

Another undesired feature produced by the new model is that although the immediate neighboring minicolumns have very different receptive fields, more distant minicolumns share similar receptive fields. As illustrated in Figure 3.5, taking the minicolumn at the upper rightmost corner of the macrocolumn as an example again, there are two minicolumns color-coded in dark-blue within a radius of two minicolumns.

The existence of similar receptive fields among non-adjacent minicolumns suggests the existence of high correlation between their activities evoked by the same point stimuli, which is confirmed by Figure 3.6 which shows the histogram of the correlations of all 1830 pairs of minicolumns in terms of their activities evoked by

the 5-point stimuli. In contrast to the histogram of the correlations of the starting state (Figure 3.3), which was almost flat and evenly distributed ranging from -0.25 to +1, the histogram of the correlations of the stable state indicates that during computer simulation a significant number of pairs of minicolumns were indeed decorrelated, resulting in a significant increase in the percentage of correlations close to 0. However, the percentage of the correlations with value 1 also increased and therefore confirmed the existence of highly correlated pairs of minicolumns, which is undesirable since we hypothesized that minicolumns in the cerebral cortex should be essentially decorrelated and independent from each other in order to reduce redundant information and achieve the maximal omnipotency in information transformation. In turn, the results obtained from the omnipotency test indicates that there was no significant improvement over the omnipotency and the omnipotency scores were nearly zero for both the starting state and the steady state, which suggest that the new model needs parameter optimization.

After searching systematically through the parameter space, we narrowed down the number of critical parameters to 3 that maximize the network's omnipotency. Figures 3.7 – 3.10 illustrate the trajectories of minicolumnar receptive field centers during the optimal development (Figure 3.7), the shuffled receptive field centers (Figures 3.8 – 3.9) and the histogram of the correlations (Figure 3.10). There were several significant improvements in the optimal model. First, the receptive field centers of all 61 minicolumns were distributed more evenly throughout the skin field rather than more towards the periphery (Figure 3.9), which was ideal and closer to the distribution of the receptive fields of real cortical neurons observed in

experiments. The receptive field centers of neighboring minicolumns were dispersed in a more complex pattern rather than the “zigzag” and the “triangles” (Figure 3.8). The pattern of the color alternation of the 61 minicolumns within the same macrocolumn represented more diversity and fewer stereotypes (Figure 3.9). In the histogram of the correlations, the percentage of the correlations with values close to 1 was zero and the majority of the correlations were close to 0. The overall profile of the histogram was closer to a normal distribution centered around 0 (Figure 3.10). The average correlation and omnipotency score were improved to 0.039 and 0.497, respectively.

We further investigated the contributions of the three critical parameters to this newly developed minicolumnar model individually, focusing on decorrelation and omnipotency. The results are illustrated in Figure 3.11 – 3.18.

First, we assessed the importance of the fixed lateral inhibition, which was included in both the 1994 Favorov-Kelly model and the new model. We varied the strength of the fixed lateral inhibition, ranging from 0 to 30, while setting all other parameters to the optimal values (Figure 3.11 – 3.12). The average correlation did clearly show the trend of descending and stabilizing roughly after the strength was more than 15, which was the optimal parameter we chose for the strength of the fixed lateral inhibition. Correspondingly, the omnipotency score increased gradually from almost 0 to 0.5 and became saturated after the strength was more than 15. Figure 3.11 – 3.12 revealed that the stronger the fixed lateral inhibition, the lower the average correlation and the higher the omnipotency score. But the overall performance was not improved significantly after the strength was more than 15.

Next, we kept all the parameters and settings the same as those in the optimal condition, but extended the radius of the fixed lateral inhibition to 2 minicolumns. The results are illustrated in Figure 3.13. There was not much difference in terms of the shuffled receptive fields except that the receptive field centers were distributed more towards the center of the skin field in this trial, while the receptive field centers were more spread out under the optimal condition. The histogram of the correlations was less ideal than the one observed with the optimal condition and the percentage of high correlations increased. Although the average correlation remained nearly zero, the omnipotency score dropped significantly from 0.497 under the optimal condition to 0.140 in this trial! These results suggest that this neural network achieves its best performance with the fixed lateral inhibition restricted to immediate neighboring minicolumns.

Next, we evaluated the importance of the Anti-Hebbian plastic lateral inhibition, which was introduced in this new model. Again, we retained the optimal parameters and settings except for varying the scaling constant controlling the strength of the Anti-Hebbian plastic lateral inhibition, ranging from 0 to 20 (Figures 3.14 – 3.15). Both the average correlation and the omnipotency score showed sharp transitions from 0 to 2 but the overall trends were similar to the ones we observed in the case of the fixed lateral inhibition previously, which suggested that even very small Anti-Hebbian plastic lateral inhibition was effective enough to decorrelate the minicolumns and improve the omnipotency of the neural network and that stronger Anti-Hebbian plastic lateral inhibition was not necessary.

Next, we moved the Anti-Hebbian plastic lateral inhibition on the proximal

compartment, while retaining all the other optimal parameters and settings. The results are illustrated in Figure 3.16. Once again, the omnipotency score dropped significantly from 0.497 under the optimal condition to 0.139 in this trial, which suggested that it was critical to place the Anti-Hebbian plastic lateral inhibition on the distal compartment.

Next, we investigated the importance of the longitudinal conductance. The results are illustrated in Figures 3.17 – 3.18, which clearly demonstrate that the larger the longitudinal conductance, the higher the average correlation and the lower the omnipotency score. Therefore, the smallest possible value of 2 was determined to be the optimal value for the longitudinal conductance. The longitudinal conductance connecting the distal compartment and the proximal compartment controlled the influence imposed from one compartment on the other. Zero longitudinal conductance separated the two compartments completely and excessively large longitudinal conductance made the two compartments behave essentially equivalent to one compartment. An effective two-compartment model is necessary to the functioning of the newly developed minicolumnar model. Separating the excitatory inputs (thalamic afferent inputs) from the fixed lateral inhibitory inputs by placing them on different compartments helps to make them more effective in the development of the thalamocortical connections and their functional properties. Therefore, the smallest possible longitudinal conductance was critical to the success of this newly developed minicolumnar model.

Lastly, in order to test the robustness of our newly developed minicolumnar model, we evaluated neurons' stimulus orientation sensitivity. The results are shown

and compared with the published results based on the 1994 Favorov-Kelly model in Figures 3.19 – 3.20. In Figure 3.19, although in the previous model we observed differential responses of an example minicolumn to a vertically-oriented bar stimulus and a horizontally oriented bar stimulus, the difference was not very big: the bar stimulus in the non-preferred orientation (horizontal) still evoked strong response. However, in the new model, most of the minicolumns are sensitive to narrow ranges of stimulus orientations. A sharp peak in orientation tuning suggests that the minicolumn responds actively only when the bar stimuli were closely aligned with its preferred orientation. Figure 3.20 demonstrates the preferred orientations in an alternative way. The results of orientation tuning obtained in the new model are closer to the experimental results observed in real cortical neurons.

Index	RM	G^L	C^{de}	C^{pi}	C^{di}	#	$aveD$	$aveC$	$Omni$	**Figure**
1	0.1	2	0.05	2	0	10	1.628	0.324	0.030	3.1 - 3.3
2	0.1	2	0.05	2	0	200	4.269	0.200	0.055	3.4 - 3.6
3	0.1	2	0	15	10	200	5.120	0.039	0.497	3.7 - 3.10, 3.13, 3.16, 3.19, 3.20

Table 3.1. Parameters used in simulations and summary of results.

RM (Rate of Maturation), G^L (Longitudinal Conductance), C^{de} (the strength of the lateral excitation placed on the distal compartment), C^{pi} (the strength of the fixed lateral inhibition placed on the proximal compartment), C^{di} (the strength of the Anti-Hebbian plastic lateral inhibition placed on the distal compartment), # (the number of connection updates), $aveD$ (the average distance between the receptive field centers of immediate neighboring minicolumns in the skin field), $aveC$ (the average correlations of activities of all 1830 pairs of minicolumns), $Omni$ (the omnipotence score of the minicolumnar network or the macrocolumn).

Index 1 refers to the starting state before connection development with equivalent parameters and settings to the 1994 Favorov-Kelly model and Figure 3.1 – 3.3.

Index 2 refers to the stable state after connection development with equivalent parameters and settings to the 1994 Favorov-Kelly model and Figure 3.4 – 3.6.

Index 3 refers to the stable state after connection development with the optimal parameters and settings and Figure 3.7 – 3.10, 3.13, 3.16, 3.19, and 3.20.

C^{pi}	*aveC*	*Omni*
0.0	0.094	0.016
2.5	0.083	0.126
5.0	0.065	0.323
7.5	0.052	0.424
10.0	0.045	0.467
12.5	0.043	0.496
15.0	0.039	0.497
17.5	0.038	0.505
20.0	0.037	0.496
22.5	0.038	0.500
25.0	0.035	0.506
27.5	0.037	0.502
30.0	0.035	0.500

Table 3.2. The strength of fixed lateral inhibition placed on the proximal compartment against average correlation and omnipotency score.
The data refers to Figure 3.11 and 3.12.

C^{di}	*aveC*	*Omni*
0	0.207	0.108
2	0.056	0.406
4	0.046	0.447
6	0.043	0.462
8	0.041	0.494
10	0.039	0.497
12	0.038	0.500
14	0.038	0.501
16	0.037	0.507
18	0.037	0.510
20	0.035	0.507

Table 3.3. The strength of Anti-Hebbian plastic lateral inhibition placed on the distal compartment against average correlation and omnipotency score.
The data refers to Figure 3.14 and 3.15.

G^L	*aveC*	*Omni*
2	0.039	0.497
4	0.044	0.462
8	0.049	0.423
16	0.057	0.368
32	0.062	0.299
64	0.065	0.271
128	0.068	0.245
256	0.069	0.234
512	0.070	0.229
1024	0.070	0.226
2048	0.070	0.225

Table 3.4. Longitudinal conductance against average correlation and omnipotency score.
The data refers to Figure 3.17 and 3.18.

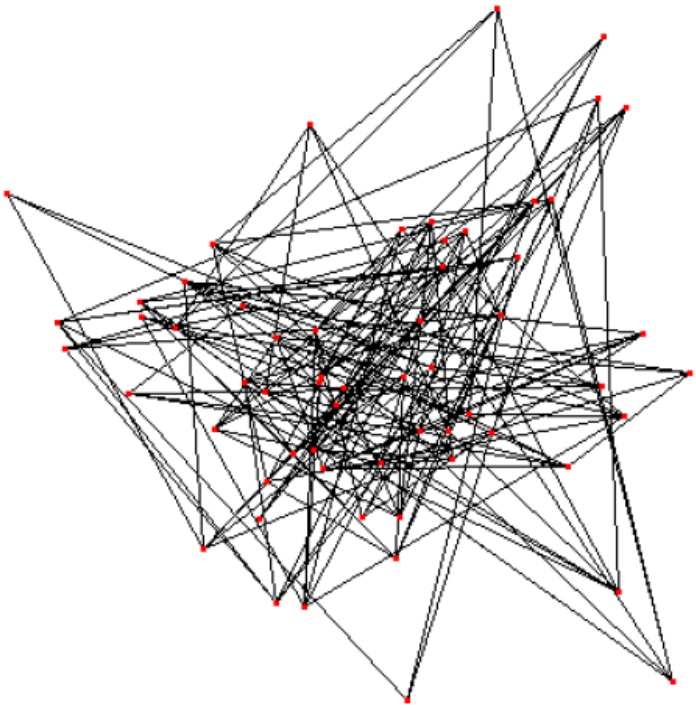

Figure 3.1. Receptive field centers of minicolumns before connection development.
Receptive field centers (red dots) of immediate neighboring minicolumns within the same macrocolumn are connected by straight lines.

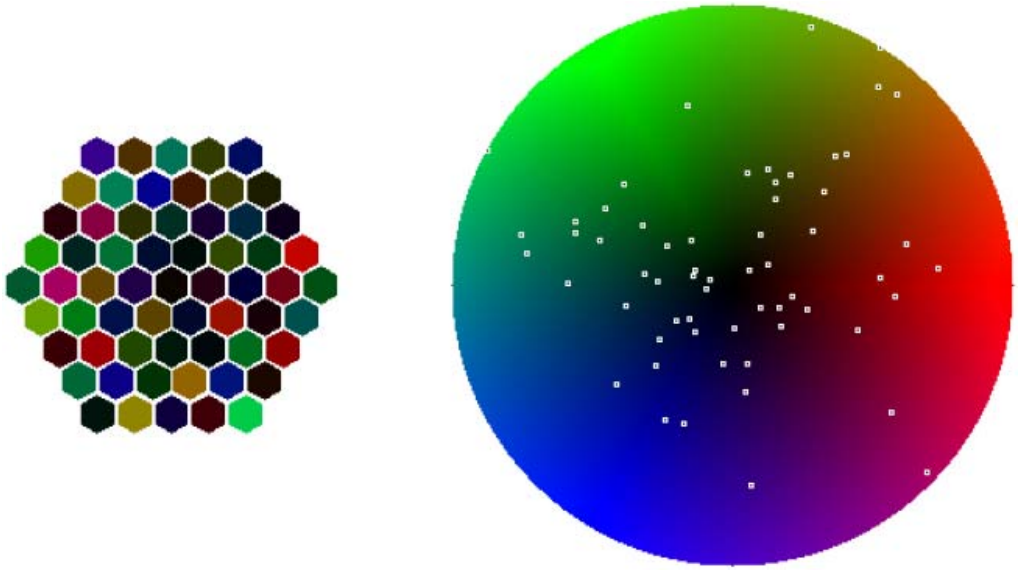

Figure 3.2. Color-coded skin field and minicolumns colored by the position of their receptive fields before connection development.
The receptive field centers (white dots) of minicolumns are dispersed in color-coded circular skin field on the right panel. On the left panel, 61 minicolumns are colored according to the color of the region where their receptive field centers locate.

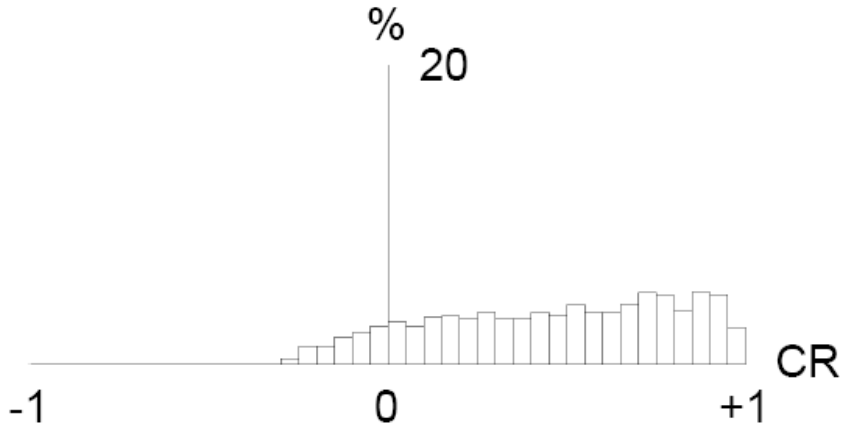

Figure 3.3. Histogram of correlations before connection development.

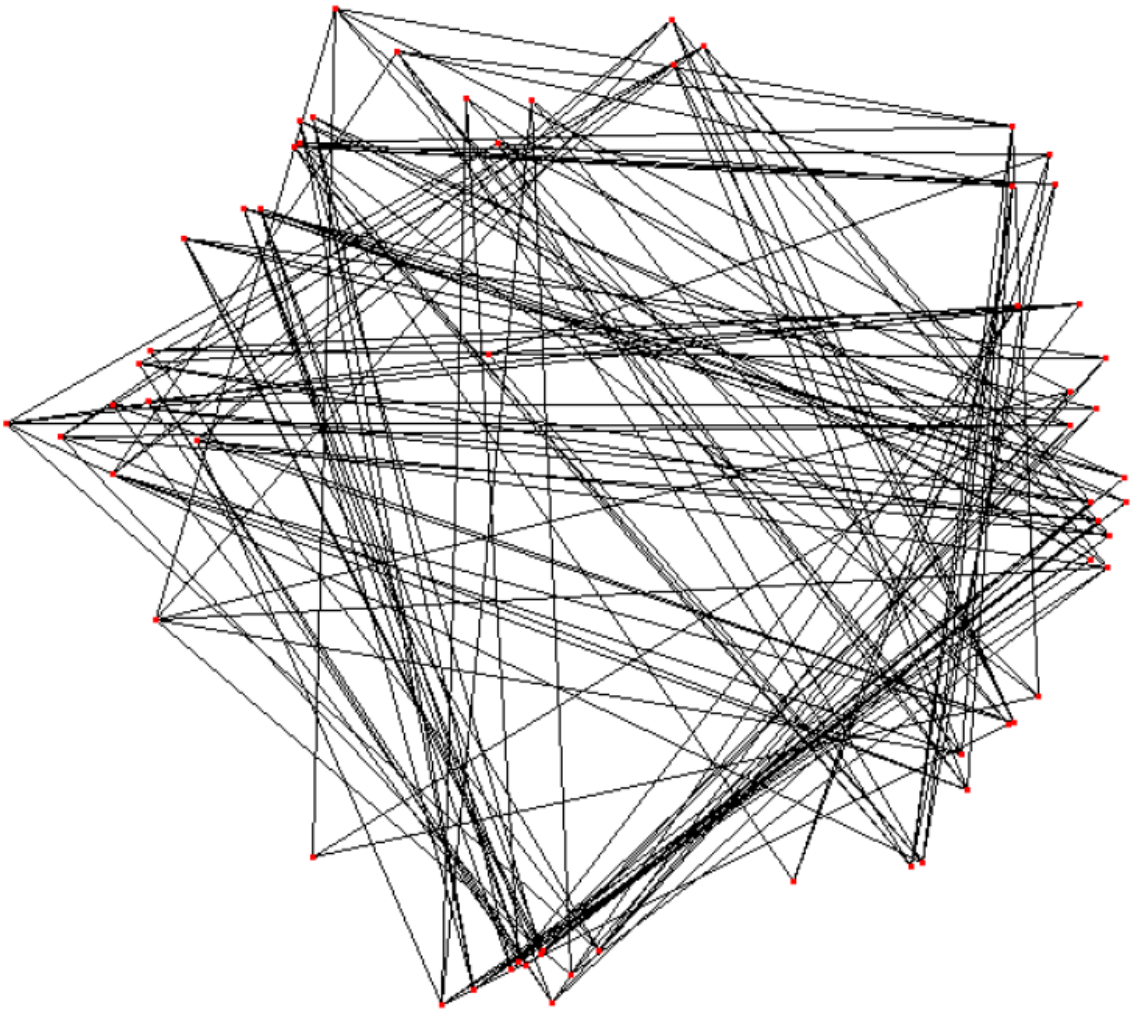

Figure 3.4. Shuffled receptive field centers of minicolumns after connection development.
Receptive field centers (red dots) of immediate neighboring minicolumns are connected by straight lines.

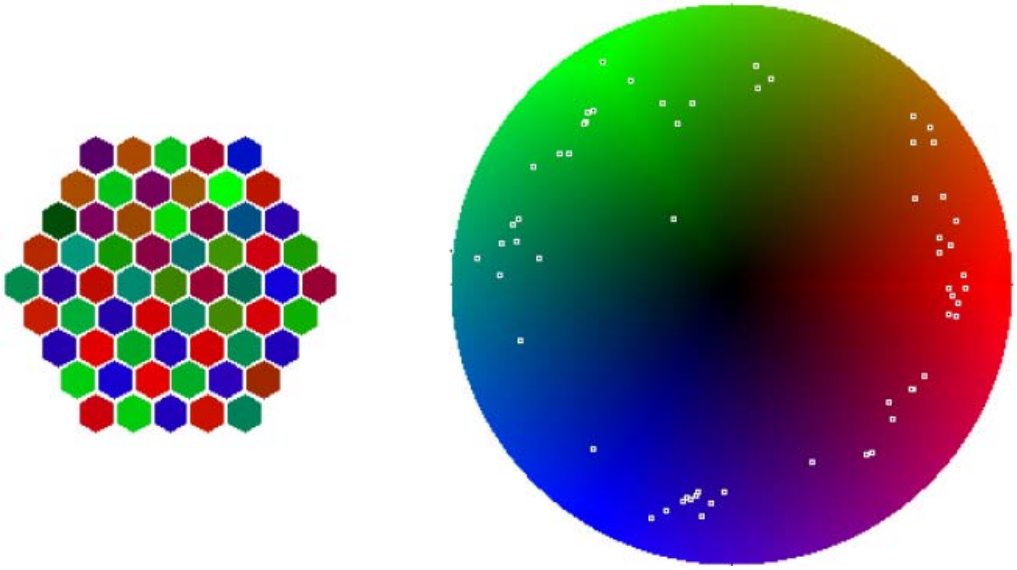

Figure 3.5. Color-coded skin field and minicolumns colored by the position of their receptive fields after connection development.
The receptive field centers (white dots) of minicolumns are shown in color-coded circular skin field on the right panel. In the left panel, 61 minicolumns are colored according to the color of the region where their receptive field centers locate.

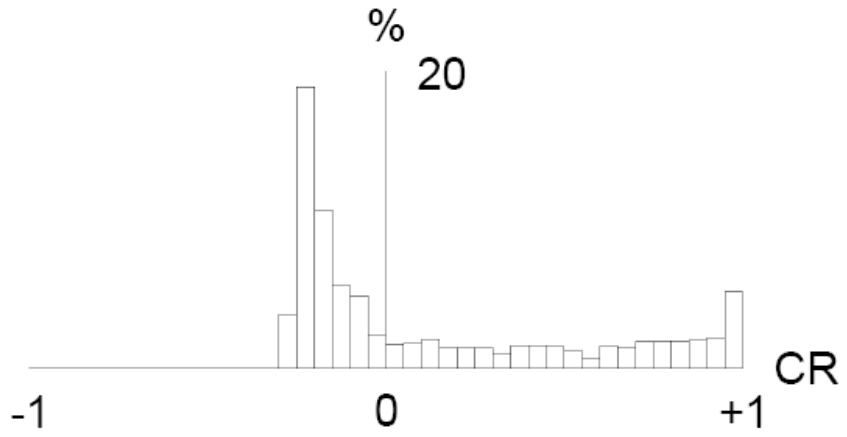

Figure 3.6. Histogram of correlations after connection development.

Figure 3.7. Trajectories of receptive field centers of minicolumns during connection development with optimal parameters and settings.

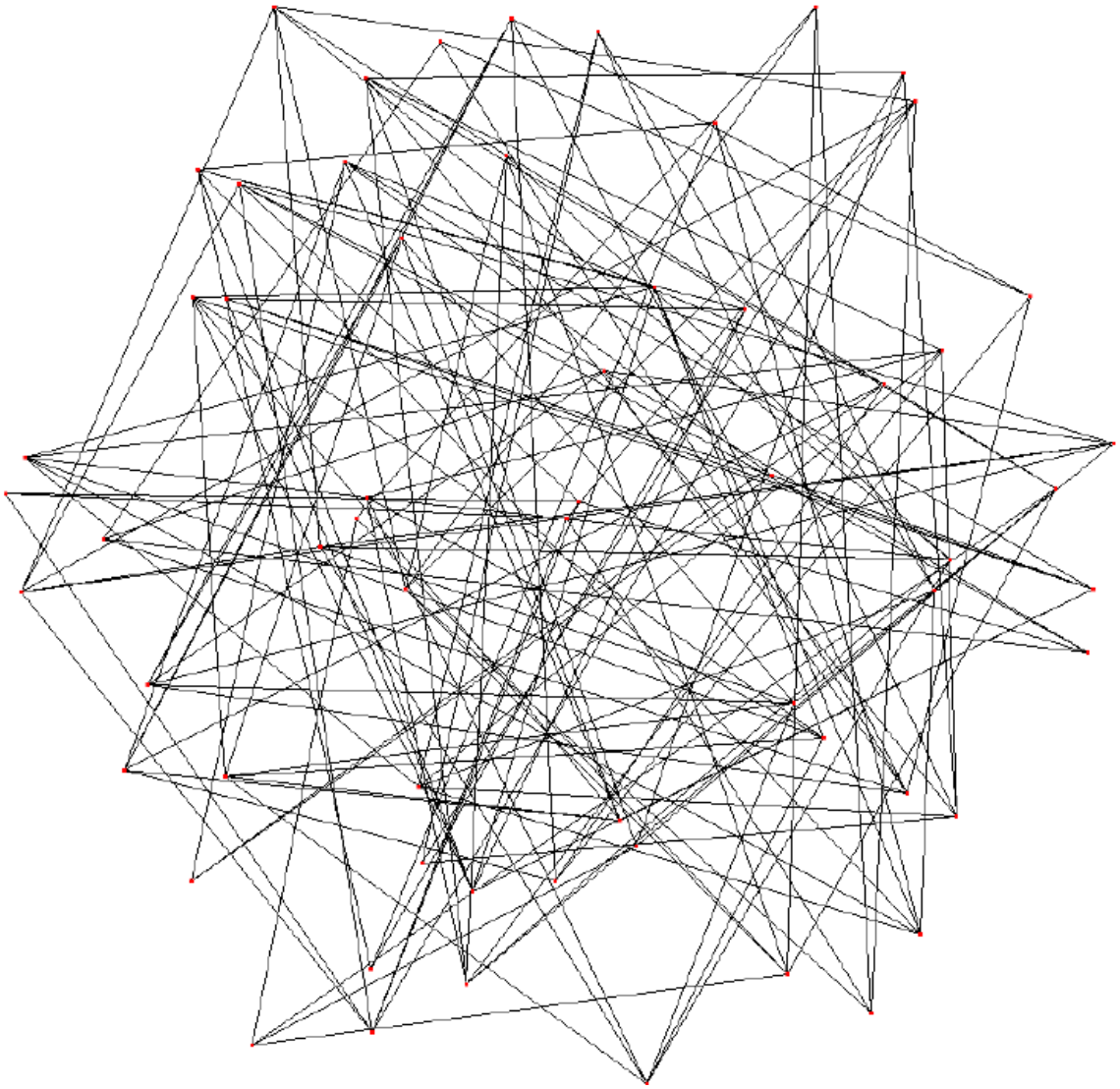

Figure 3.8. Shuffled receptive field centers of minicolumns after connection development with optimal parameters and settings.

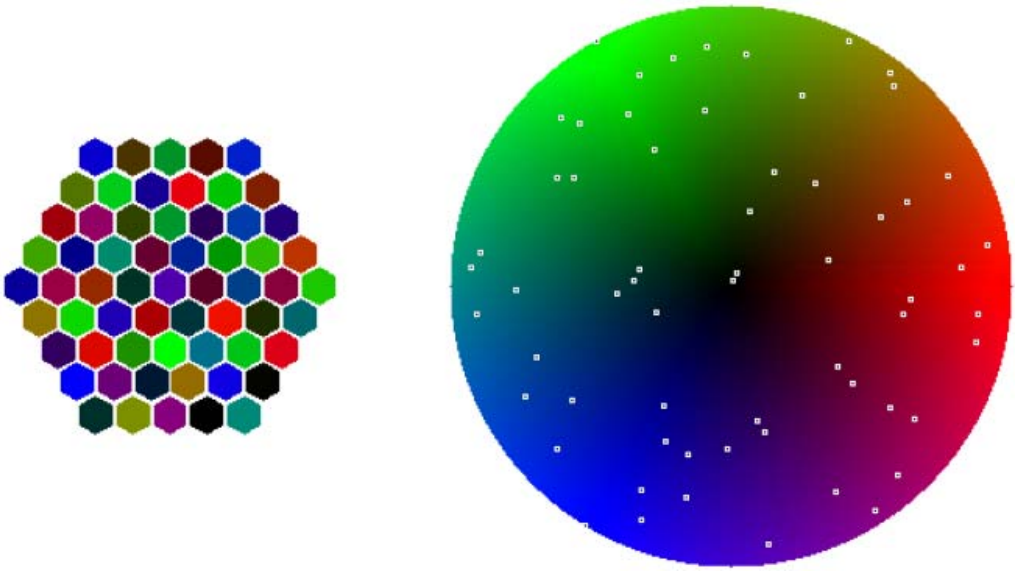

Figure 3.9. Color-coded skin field and minicolumns colored by the position of their receptive fields after connection development with optimal parameters and settings.

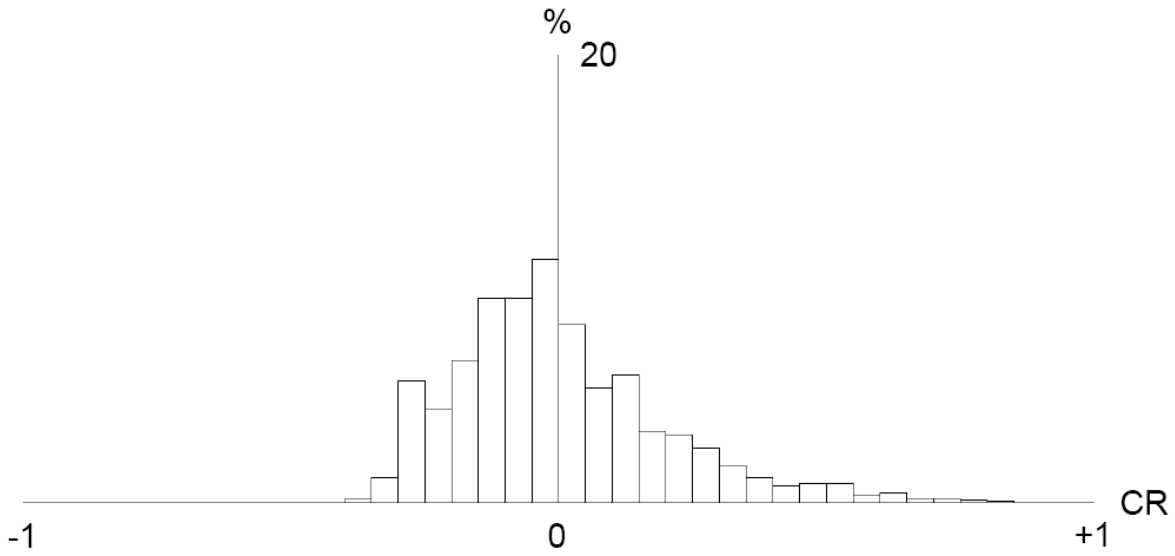

Figure 3.10. Histogram of correlations after connection development with optimal parameters and settings.

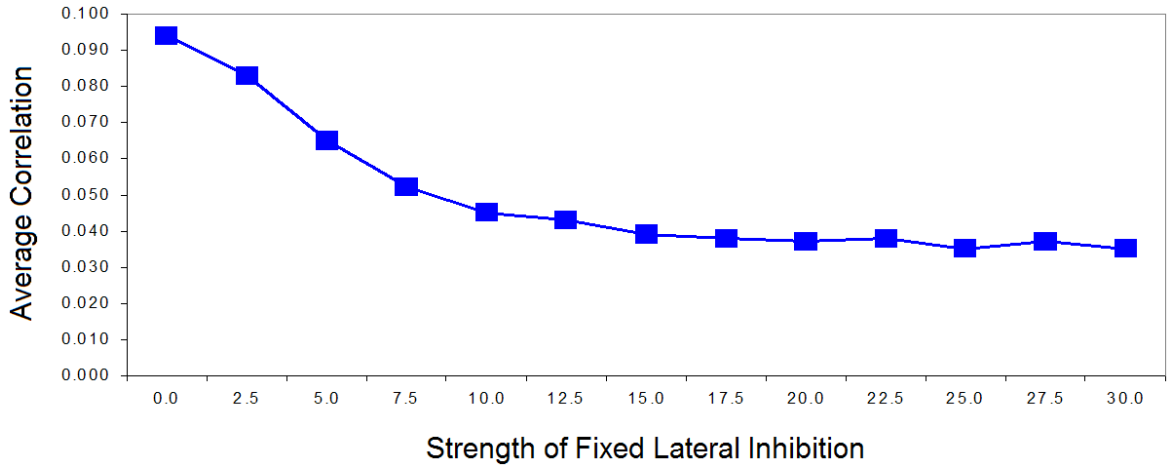

Figure 3.11. Average correlation plotted against fixed lateral inhibition strength.

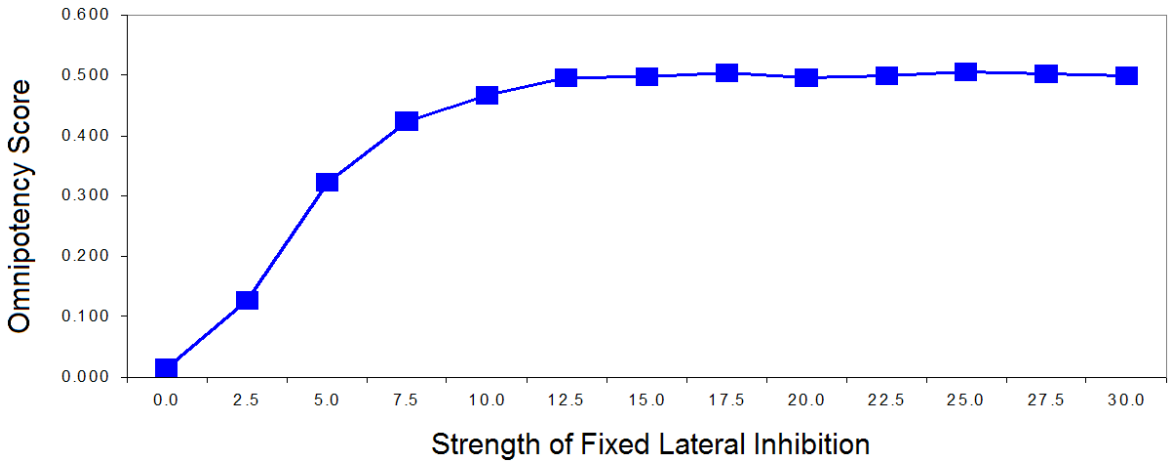

Figure 3.12. Omnipotency score plotted against fixed lateral inhibition strength.

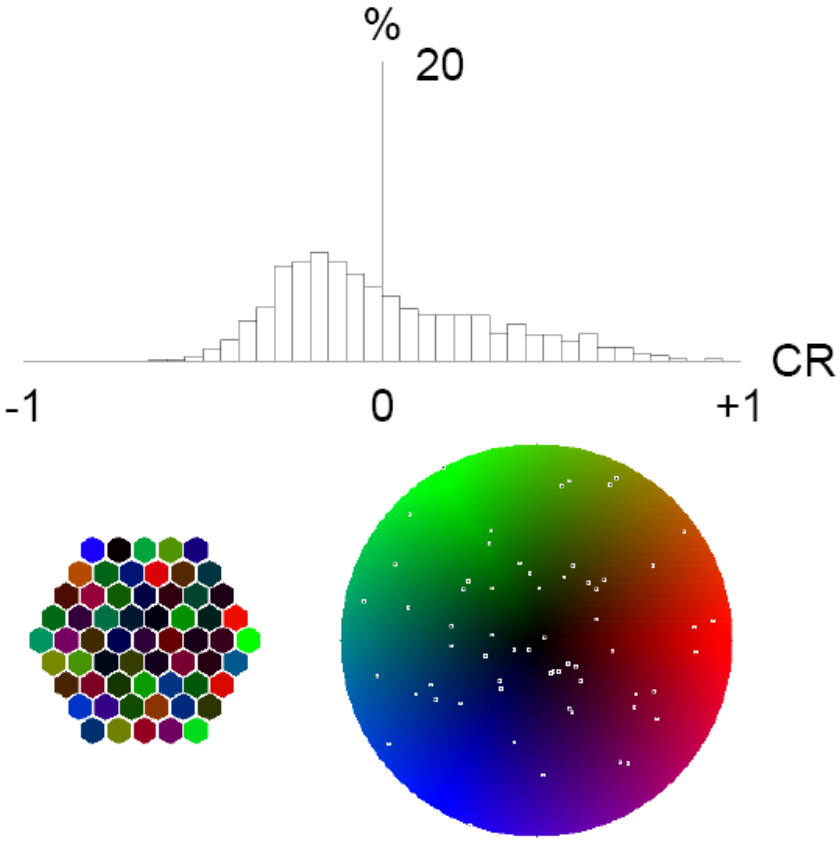

Figure 3.13. Fixed lateral inhibition is extended to a radius of 2 minicolumns. All the other optimal parameters and settings are retained. The resulting histogram of the correlations (CR) of 1830 pairs of minicolumns is plotted in the upper panel. The resulting color-coded skin field and minicolumns reflecting the shuffled receptive fields of minicolumns after connection development are plotted in the lower panel.

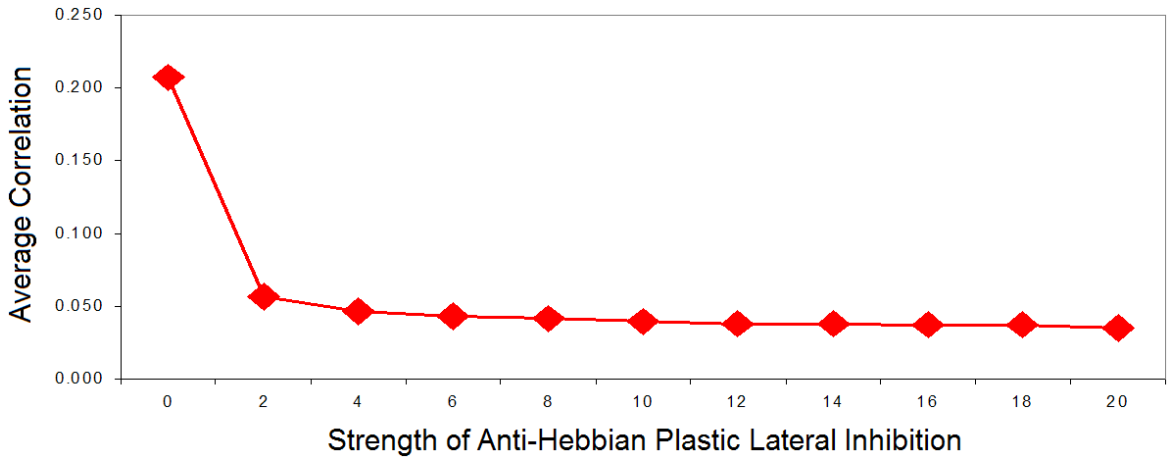

Figure 3.14. Average correlation plotted against Anti-Hebbian plastic lateral inhibition strength.

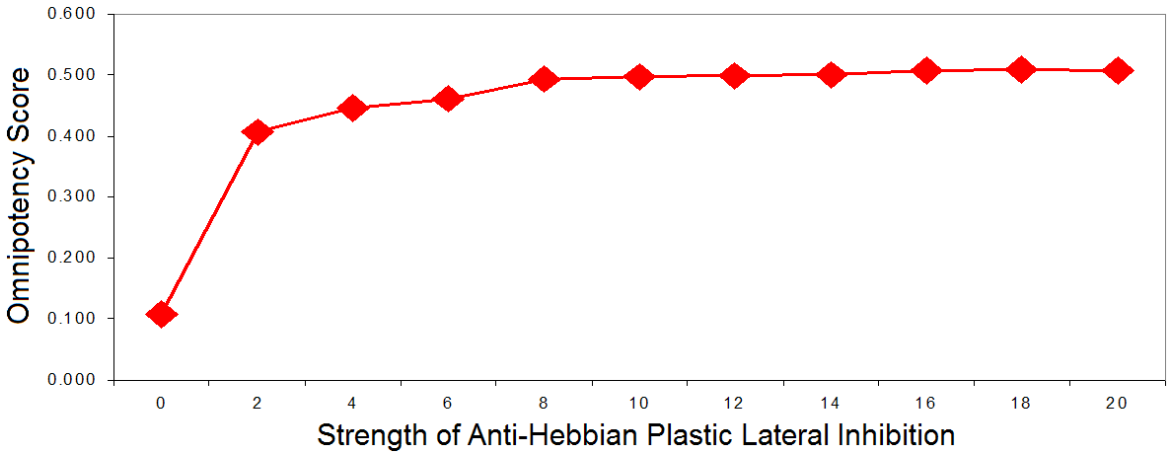

Figure 3.15. Omnipotency score plotted against Anti-Hebbian plastic lateral inhibition strength.

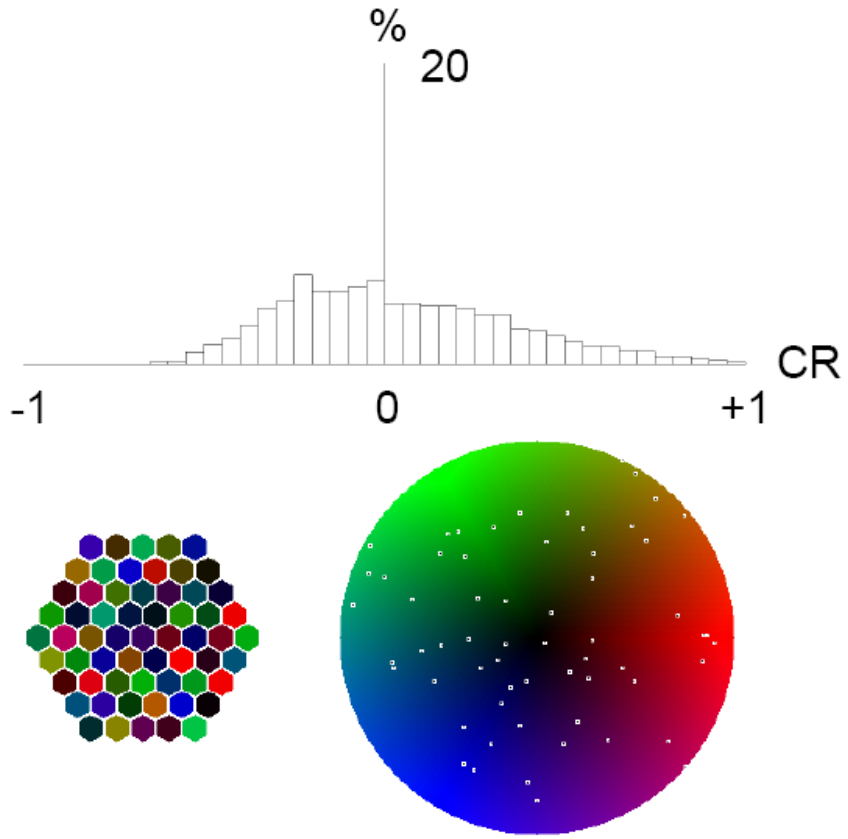

Figure 3.16. Anti-Hebbian plastic lateral inhibition is placed in the proximal compartment.
All the other optimal parameters and settings are retained. The resulting histogram of the correlations (CR) of 1830 pairs of minicolumns is plotted in the upper panel. The resulting color-coded skin field and minicolumns reflecting the shuffled receptive fields of minicolumns after connection development are plotted in the lower panel.

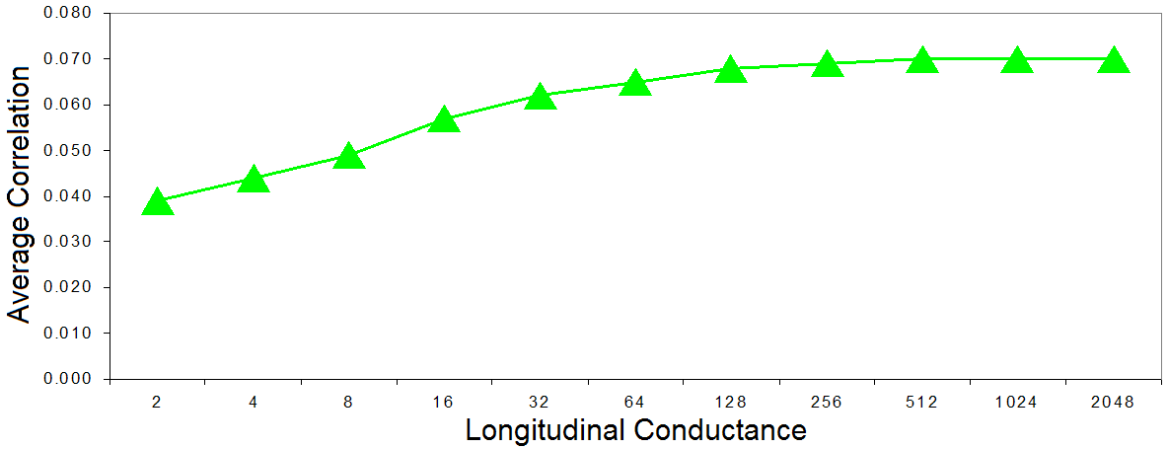

Figure 3.17. Average correlation plotted against longitudinal conductance.

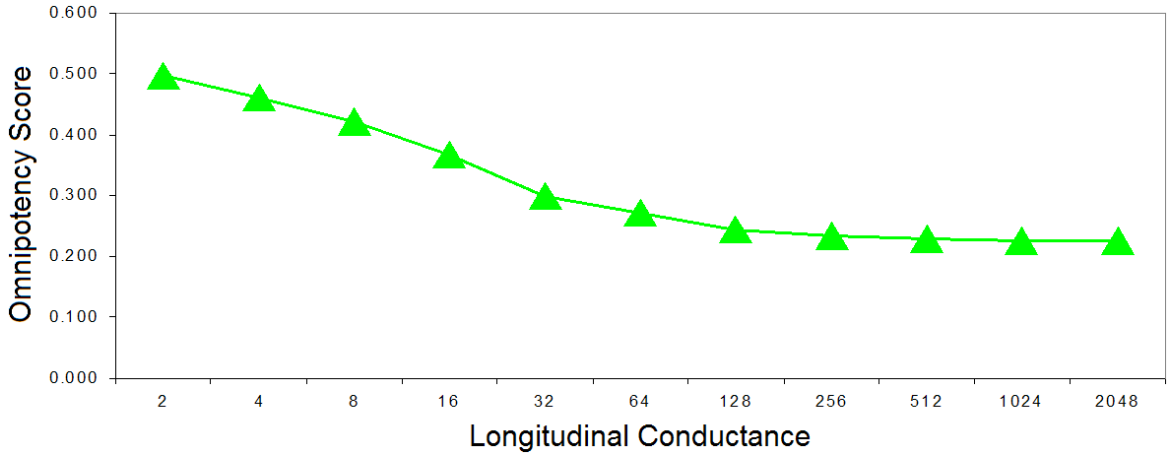

Figure 3.18. Omnipotency score plotted against longitudinal conductance.

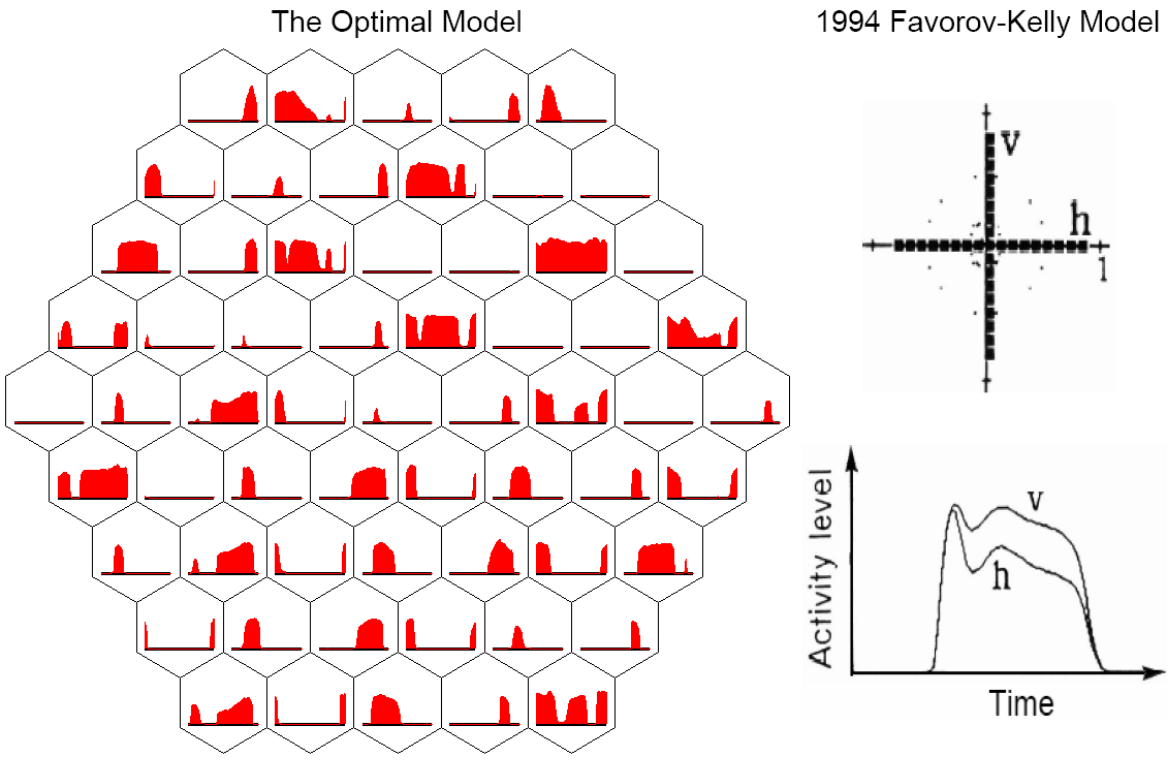

Figure 3.19. Orientation tuning plot 1.
Based on 1994 Favorov-Kelly model, activities of an exemplary simulated minicolumn in response to vertically oriented bar stimulus and horizontally oriented bar stimulus are shown in the right panel (Favorov and Kelly, 1994 b). Although there is observable difference in the activity level of simulated minicolumn, the unfavorable horizontal bar stimulus still activates the minicolumn. In the left panel, based on the new model with the optimal parameters and settings, most simulated minicolumns demonstrate high sensitivity to narrow range of orientations.

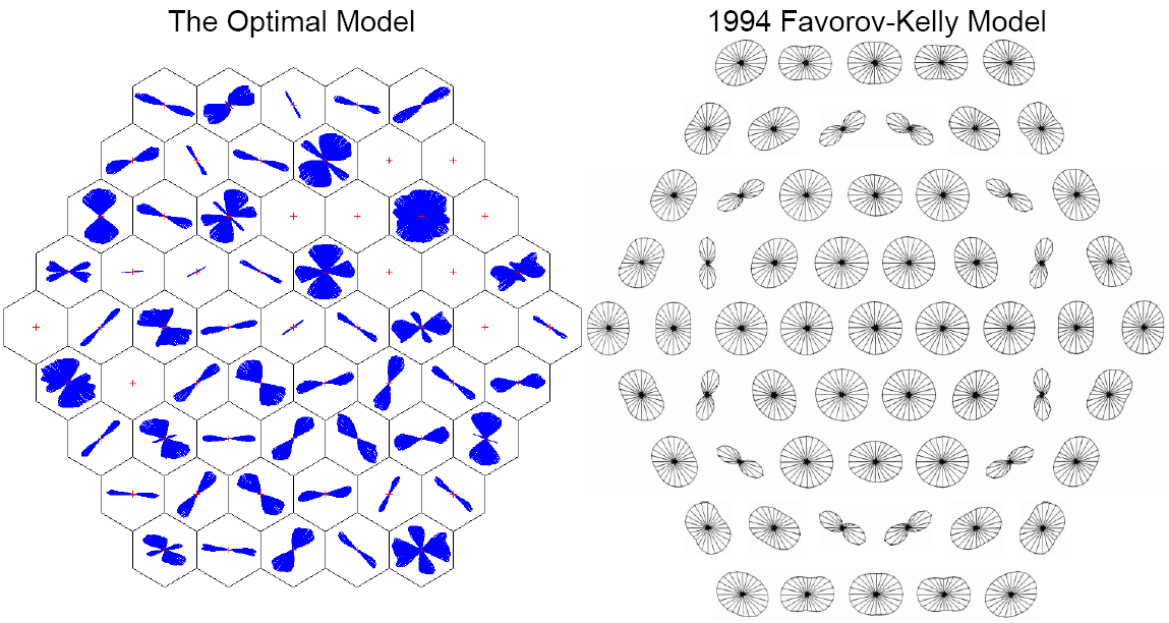

Figure 3.20. Orientation tuning plot 2.
For each minicolumn, line stimuli centered at its receptive field center with different orientations are across its entire receptive field. Not only those line stimuli are plotted but also the length of each line stimulus is scaled according to the minicolumnar activity evoked by it. There exists more diversity in orientation tuning in simulated minicolumns based on the new model with the optimal parameters and settings than in the 1994 Favorov-Kelly model (Favorov and Kelly, 1994b).

CHAPTER 4

DISCUSSIONS

In this dissertation work, we developed a dynamic system to approximate the layer 4 cortical network based on the 1994 Favorov-Kelly model. We simplified the original model, placing emphasis on lateral inhibition. With this setup, we successfully reproduced some characteristic features observed in real cortical networks, such as shuffled receptive fields and emergence of prominent orientation tuning. After numerous trials with a large variety of parameter settings, we finally narrowed down the number of critical parameters to 3. These parameters were: (1) the strength of the fixed lateral inhibition applied on the proximal compartment, (2) the existence of the Anti-Hebbian plastic lateral inhibition imposed on the distal compartment, and (3) the small longitudinal conductance between the proximal compartment and the distal compartment of the modeled minicolumn-representing neuron. Under the optimal condition, defined by the maximal omnipotence in the neural network, the system achieves nearly zero average correlation between any pair of its neurons, prominent receptive field shuffling, and well-developed higher-level feature sensitivities.

The reason why the two-compartment design of modeled neurons was necessary to the successful functioning of the system is as follows. Since the system was expected to be able to reproduce some heterogeneous characteristics observed

in the real cortical neurons and the characteristics of the model neuron were determined at least in part by its thalamocortical connections, the lateral inhibition must exist among the model neurons because of its influence on the development of the thalamocortical connections. The existence of the lateral inhibition among the model neurons forces each of them to develop different sets of thalamocortical connections, resulting in receptive field positional heterogeneity. However, the development of the thalamocortical connections primarily follows the Hebbian Rule. If we adopted a one-compartment neuron model, the thalamocortical connections of a neuron would continue to change until its excitatory thalamic input is balanced with its inhibitory lateral input. At its full development, the excitation would cancel out the inhibition completely. Therefore, in a one-compartment model, the development of the thalamocortical connections following the Hebbian Rule eventually neutralizes the impact of the lateral inhibition in shaping the properties of the output. But by adopting a two-compartment model and separating the excitatory input from the inhibitory lateral input, a win-win situation could be achieved. In order to approximate real cortical neurons, the excitatory thalamic afferent input was placed on the distal compartment and the inhibitory lateral input was arranged on the proximal compartment. The influence imposed on one compartment from the other compartment was controlled by the longitudinal conductance between the proximal compartment and the distal compartment. The larger the longitudinal conductance, the more comparable the behavior of the two-compartment model was to that of the one-compartment model. The smaller the longitudinal conductance, the less the influence was imposed on the state of the distal compartment, dominated by the

excitatory thalamic afferent input, by the state of the proximal compartment, dominated by the inhibitory lateral input. Therefore, with a small enough longitudinal conductance between the two compartments, the two-compartment model can satisfy our design requirements for the model neuron. That is, in the distal compartment, the thalamocortical connections were developed following the Hebbian Rule based on the correlation of the activities of the presynaptic cell and the postsynaptic cell; meanwhile, in the proximal compartment, the lateral inhibition was predominant and capable of shaping the functional properties of the model neuron.

Results of computer simulations of the model presented in Chapter 3 demonstrate the importance of the lateral inhibition in improving the performance of the neural network in decorrelation and omnipotence. But why the fixed lateral inhibition had to be placed on the proximal compartment and restricted locally between the immediate neighboring neurons, while the Anti-Hebbian plastic lateral inhibition had to be placed on the distal compartment and link all pairs of minicolumns in the macrocolumn? First of all, the closer the inhibitory input is to the output, the more effective the inhibition is. The fixed lateral inhibition between two immediate neighboring minicolumns could sculpt their receptive fields to certain nonlinear features. For example, as illustrated in Figure 4.1, we assumed that the thalamocortical connections of two hypothetical neurons had already reached the steady state and the profile of their receptive fields in a unidimensional state space is gaussian. In addition, these two neurons have largely overlapping receptive fields. If there were no lateral inhibition between them, their receptive fields would maintain

gaussian profiles (shown by the red dashed line and the blue dashed line, respectively, in Figure 4.1). However, if there was fixed lateral inhibition between them, their receptive fields would be significantly altered, as indicated by the red solid line and the blue solid line, respectively, in Figure 4.1, and their receptive field profiles are no longer gaussian. A nearly complete inhibitory region is produced between the excitatory regions of these two neurons, thereby creating a new feature sensitivity.

The Anti-Hebbian plastic lateral inhibition between all pairs of the model minicolumns helps to shuffle the receptive fields of the minicolumns across the entire macrocolumn more thoroughly. As pointed out in Chapter 3, with the fixed lateral inhibition between immediately neighboring minicolumns alone, the shuffled receptive field centers of minicolumns were distributed in a “zigzag” pattern and there were pairs of minicolumns which were highly correlated in response to skin stimuli, resulting in lower performance in omnipotence. With the assistance from the Anti-Hebbian lateral inhibition between all pairs of minicolumns, they all become more or less decorrelated. Because the receptive field of a minicolumn was determined primarily by the thalamocortical connections, the Anti-Hebbian plastic lateral inhibitory input was placed on the distal compartment together with the excitatory thalamic afferent input to participate in selection of the thalamocortical connections. In turn, it improved not only the decorrelation but also the omnipotence of the neural network, as demonstrated in Chapter 3.

The biological identities of the structural features of this newly developed neural network are suggested in Figure 4.2. Since the spiny stellate cell is the

predominant excitatory cell type in the input cortical layer 4, receiving the thalamic afferent input and then relaying it to cells in the other cortical layers. The two-compartment model neuron can be identified with the spiny stellate cell in the layer 4. Two other types of cortical cells are very likely candidates to provide the lateral inhibition. They are the chandelier cell (Peters, 1984) and the basket cell (Jones and Hendry, 1984). The chandelier cell synapses exclusively on the initial segment of the axon of the excitatory cortical cells, which renders it the most effective inhibitory cell in the cerebral cortex. In addition, the layer 4 chandelier cells inhibit only neighboring cortical cells due to their relatively confined axonal branches. Therefore, the cell providing the fixed lateral inhibition locally in our model can be identified with the chandelier cell. The basket cells exist in all cortical layers and synapse on both dendrites and somata of the cortical cells in a much wider spatial range due to their relatively large macrocolumn-sized axon arbor. Therefore, the cell providing the Anti-Hebbian plastic lateral inhibition in our model can be identified with the basket cell. Accordingly, the biological identities of the distal and proximal compartments in the new model are not the same as in the 1994 Favorov-Kelly model. In the 1994 Favorov-Kelly model, the distal compartment and the proximal compartment were referred to the dendrites and the soma of the spiny stellate cell, respectively. But in this new model, the proximal compartment is identified with the initial axon segment of the spiny stellate cell, and the distal compartment is identified with the dendrites and soma of the spiny stellate cell.

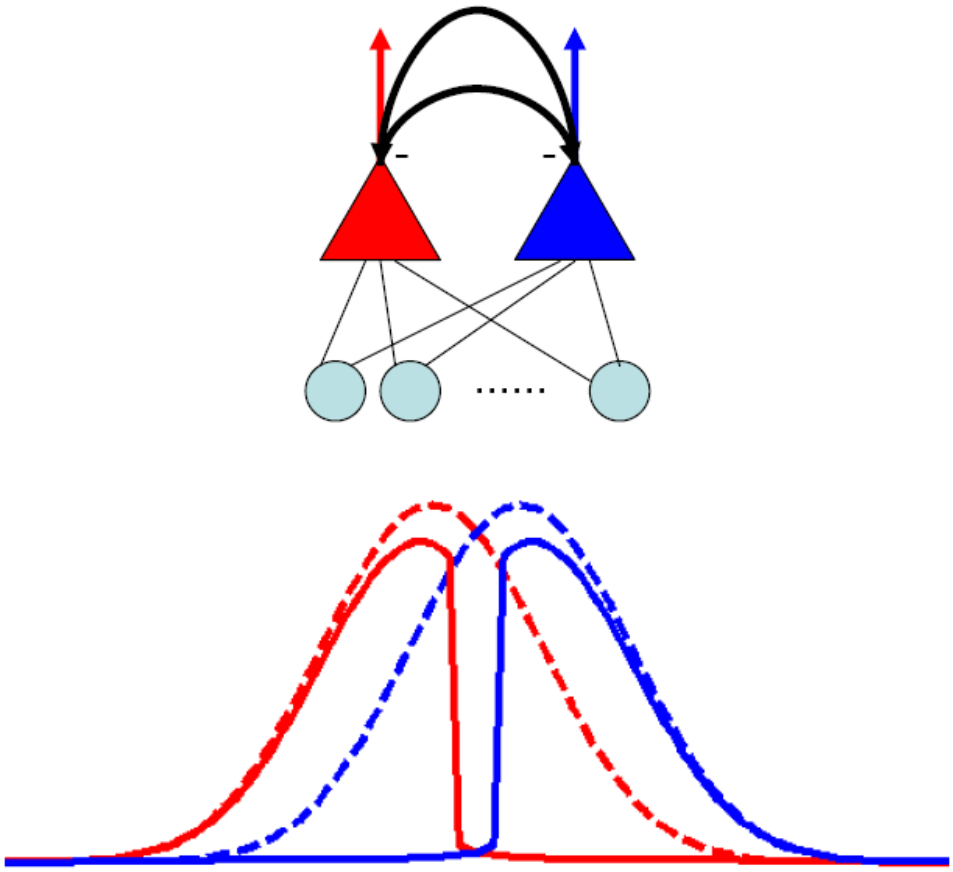

Figure 4.1. Mutual fixed lateral inhibition between two neighboring cortical neurons with largely overlapped receptive fields.
Two cortical neurons (denoted by red and blue solid triangles) with fully developed connections with thalamic neurons (denoted by Carolina blue solid circles) have largely overlapped unidimensional receptive fields. Their receptive field profiles are gaussian and distinguished by red and blue dashed lines, if there is no mutual lateral inhibition between them. If there is mutual fixed lateral inhibition between them (denoted by black arrows and negative signs close to arrow heads), the receptive field profiles are significantly alternated and distinguished by red and blue solid lines. In addition, a nearly completely inhibitory region between their excitatory regions is produced.

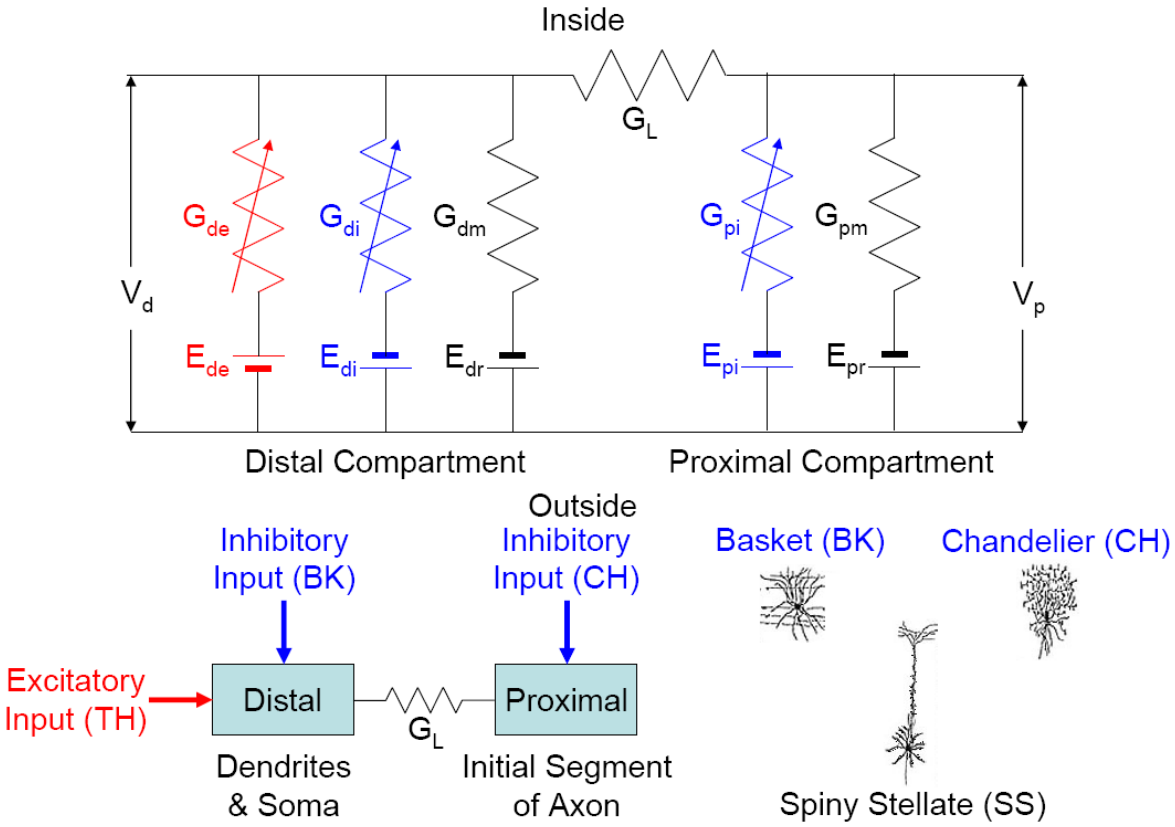

Figure 4.2. Biological identities of the new minicolumnar model.
We suggest that the biological identities referred to our new minicolumnar model are as follows. The two-compartmental neuronal model refers to the spiny stellate cell. The distal compartment refers to dendrites and soma of the spiny stellate cell. The proximal compartment refers to the initial segment of the axon of the spiny stellate cell. The basket cell provides Anti-Hebbian plastic lateral inhibition on dendrites and soma of the spiny stellate cell (the distal compartment). The chandelier cell provides fixed lateral inhibition on the initial segment of the axon of the spiny stellate cell (the proximal compartment).

CHAPTER 5

CONCLUSIONS AND FUTURE DIRECTIONS

In this dissertation project we developed a simplified layer 4 minicolumnar model based on the 1994 Favorov-Kelly model, emphasizing the lateral inhibition. In this model we not only successfully reproduced the shuffled receptive fields and other characteristic features of cortical layer 4 neurons observed previously, but also further established the importance and the precise organization of the lateral inhibition, especially the strong fixed lateral inhibition, in decorrelating cortical neurons, introducing nonlinearity and maximizing omnipotence. The Anti-Hebbian plastic lateral inhibition among cortical neurons was found to be also critical to the performance of the neural network. The small longitudinal conductance was found to be necessary in our two-compartmental model of the cortical neuron. Finally, we suggested the most likely biological identities for each component of this model. That is, the spiny stellate cell receives its excitatory thalamic afferent input and Anti-Hebbian plastic lateral inhibitory input from basket cells on its dendrites and soma (which are referred to as the distal compartment in the model), and it receives its strong fixed lateral inhibitory input from chandelier cells on its initial axon segment (which is referred to as the proximal compartment in the model).

The core of this newly developed model is the importance of strong lateral inhibitory interactions among layer 4 neurons in adjacent minicolumns. Therefore,

the first priority must be given to seeking the actual experimental evidence to demonstrate that direct activation of spiny stellate cells in one minicolumn significantly inhibits spiny stellate cells in adjacent minicolumns.

We are also planning to further investigate the capabilities of the model to handle more natural stimulus patterns, such as images, instead of randomly picked 5-point stimuli. Since we already have a well-developed model of a single macrocolumn, we are now in a position to build a larger-scale neural network composed of multiple macrocolumns and simulate their interactions.

My dissertation work is only part of a bigger and ambitious effort focusing on unveiling the mystery of information transformation in the cerebral cortex. How the information is being further processed in the higher output layers is the next big question. We humbly believe we are on the right track.

APPENDIX – SOURCE CODE IN MATLAB

honeycomb.m

This program will return the total number of minicolumns and the coordinates of centers of minicolumns, given the number of minicolumns along one side of a macrocolumn of which the center coordinate is (0, 0).

```
function [coor num] = honeycomb(N)

num = (((N+(N*2-1))*N)/2)*2-(N*2-1);

coor = zeros(num, 2);

constantHeight = sqrt(0.75);

start = 1;
inc = N-1;
for i = 1 : 1 : (N*2-1)
    if ((i > 1) && (i <= (N+1)))
        inc = inc+1;
        start = start+inc;
    elseif (i > (N+1))
        inc = inc-1;
        start = start+inc;
    end
    if (i <= N)
        coor(start, :) = [(0-((N-1)+(i-1))*0.5), (0+((N-1)-(i-
1))*constantHeight)];
        for j = 1 : 1 : ((N-1)+(i-1))
            coor(start+j, :) = [(coor(start, 1)+j), coor(start, 2)];
        end
    elseif (i > N)
        coor(start, :) = [(0-(N-1)+(i-N)*0.5), (0-(i-N)*constantHeight)];
        for j = 1 : 1 : (((2*N-1)-1)-(i-N))
            coor(start+j, :) = [(coor(start, 1)+j), coor(start, 2)];
        end
    end
end

end
```

main.m

```
clear;
clc;
format long g;
```

```
rand('twister', 5489);

[coorMC numMC] = honeycomb(5);

[coorTH numTH] = honeycomb(7);

setExd = zeros(numMC, numMC);
setInhp = zeros(numMC, numMC);
setInhd = zeros(numMC, numMC);
for i = 1 : 1 : numMC
    temp = sqrt(sum((coorMC-ones(numMC, 1)*coorMC(i, :)).^2, 2));
    setExd(:, i) = temp < 2.5;
    setExd(i, i) = 0;
    setInhp(:, i) = temp < 1.5;
    setInhp(i, i) = 0;
    setInhd(i, i) = 0;
end

Wth_mc = rand(numTH, numMC);
Cth_mc = ones(numTH, numMC);
Wth_mc = (Wth_mc./(ones(numTH, 1)*sum(Wth_mc))).*Cth_mc;

numTimeStep = 50;
FmaxTH = 1;
rfrTH = 3;
numUpdates = 200;
counterP = 1000;
num = 5;
Cth = 1.5;
Tau = 4;
Cexd = 0;
Cinhp = 15;
Cinhd = 10;
Gl = 2;
RM = 0.1;
Fth_mc = 0.075;

force = 0.1 : 0.1 : (numTimeStep*0.1);
force = force.*(force < 1)+(force >= 1);

N = 3;
[coorTemp numTemp] = honeycomb(15*N);
coorTemp = coorTemp/N;
numP = 0;
for i = 1 : 1 : numTemp
    activityTH = sqrt(sum((coorTH-ones(numTH, 1)*coorTemp(i, :)).^2,
2))*(((-1)*FmaxTH)/rfrTH)+FmaxTH;
    if (size(find(activityTH > 0), 1) > 0)
        numP = numP+1;
        activity(numP, 1) = numP;
        activity(numP, 2 : 3) = coorTemp(i, :);
        activity(numP, 4) = 1;
        activity(numP, 5 : 4+numTH) = (activityTH.*(activityTH > 0))';
    end
```

```
end

for update = 1 : 1 : numUpdates

    temp = round(rand(counterP, num)*numP);
    temp = temp+(temp <= 0);
    activityPattern = zeros(counterP, numTH);
    for i = 1 : 1 : counterP
        for j = 1 : 1 : num
            activityPattern(i, :) = activityPattern(i, :)+activity(temp(i,
j), 5 : 4+numTH);
        end
    end

    FMCFinal = zeros(numMC, counterP);
    Vd = zeros(numMC, counterP);
    for iP = 1 : 1 : counterP
        Gexd = zeros(numMC, 2);
        Ginhp = zeros(numMC, 2);
        Ginhd = zeros(numMC, 2);
        FMC = zeros(numMC, 2);
        inputTH = (((activityPattern(iP, :)*Wth_mc)')*force)*Cth;
        for i = 1 : 1 : numTimeStep
            Gexd(:, 2) = (1-(1/Tau))*Gexd(:, 1)+(1/Tau)*(inputTH(:,
i)+Cexd*(setExd*FMC(:, 1)));
            Ginhp(:, 2) = (1-(1/Tau))*Ginhp(:,
1)+(1/Tau)*(Cinhp*(setInhp*FMC(:, 1)));
            Ginhd(:, 2) = (1-(1/Tau))*Ginhd(:,
1)+(1/Tau)*(Cinhd*(setInhd*FMC(:, 1)));
            Vp = (Gl*Gexd(:, 1))./((Gexd(:, 1)+Ginhd(:, 1)+1).*(Ginhp(:,
1)+Gl+1)+Gl*(Ginhp(:, 1)+1));
            if (i == numTimeStep)
                Vd(:, iP) = (Gexd(:, 1).*(Ginhp(:, 1)+Gl+1))./((Gexd(:,
1)+Ginhd(:, 1)+1).*(Ginhp(:, 1)+Gl+1)+Gl*(Ginhp(:, 1)+1));
            end
            FMC(:, 2) = (Vp.^3)./(0.01+(Vp.^3));
            Gexd(:, 1) = Gexd(:, 2);
            Ginhp(:, 1) = Ginhp(:, 2);
            Ginhd(:, 1) = Ginhd(:, 2);
            FMC(:, 1) = FMC(:, 2);
        end
        FMCFinal(:, iP) = FMC(:, 2);
    end

    temp = corr(activityPattern, Vd');
    Wth_mc = Wth_mc*(1-RM)+(sign(temp).*(temp.^2))*RM;
    Wth_mc = Wth_mc.*(Wth_mc > 0);
    Cth_mc = (1-RM)*Cth_mc+RM*(((Fth_mc*ones(numTH, numMC))./(ones(numTH,
1)*((mean(FMCFinal, 2))'))).*Cth_mc);
    Wth_mc = (Wth_mc./(ones(numTH, 1)*sum(Wth_mc))).*Cth_mc;

    temp = corr(Vd', FMCFinal');
    for i = 1 : 1 : numMC
        temp(i, i) = 0;
    end
    setInhd = (1-RM)*setInhd+RM*temp;
```

```
    setInhd = setInhd.*(setInhd > 0);
    for i = 1 : 1 : numMC
        setInhd(i, i) = 0;
    end

end

corrMC = corr(FMCFinal');
temp = corrMC.*(corrMC > 0);
for i = 1 : 1 : numMC
    temp(i, i) = 0;
end
temp = temp.^2;
aveCorrMC = mean(temp(:));
display(num2str(aveCorrMC, '%4.3f'));

figure;
xlim([-1 1]);
hold on;
grid on;
hist(corrMC(:), 100);

temp = sum(Wth_mc);
temp = (temp > 0).*temp+(temp <= 0)*0.001;
newCoorMC = ((Wth_mc')*coorTH)./((temp')*ones(1, size(coorTH, 2)));

counterLine = 0;
for i = 1 : 1 : numMC
    if ((abs(newCoorMC(i, 1)) < 100) && (abs(newCoorMC(i, 2)) < 100))
        temp = find(setInhp(i, :) == 1);
        for j = 1 : 1 : size(temp, 2)
            if ((abs(newCoorMC(temp(1, j), 1)) < 100) &&
(abs(newCoorMC(temp(1, j), 2)) < 100))
                counterLine = counterLine+1;
                distance(counterLine) = sqrt(sum((newCoorMC(i, :)-
newCoorMC(temp(1, j), :)).^2));
            end
        end
    end
end
aveDistance = mean(distance);
display(num2str(aveDistance, '%4.3f'));

figure;
axis equal;
xlim([-5 5]);
ylim([-5 5]);
hold on;
grid on;
for i = 1 : 1 : numMC
    if ((abs(newCoorMC(i, 1)) < 100) && (abs(newCoorMC(i, 2)) < 100))
        temp = find(setInhp(i, :) == 1);
        for j = 1 : 1 : size(temp, 2)
            if ((abs(newCoorMC(temp(1, j), 1)) < 100) &&
(abs(newCoorMC(temp(1, j), 2)) < 100))
                plot([newCoorMC(i, 1), newCoorMC(temp(1, j), 1)], ...
```

```
                    [newCoorMC(i, 2), newCoorMC(temp(1, j), 2)], 'k');
            end
        end
    end
end
plot(newCoorMC(:, 1), newCoorMC(:, 2), 'ro', 'MarkerFaceColor', 'r',
'MarkerSize', 5);

data = zeros(numMC, 180);

for indexMC = 1 : 1 : numMC

    activityPattern = zeros(180, numTH);
    counterP = 0;
    for angle = 0 : 1 : 179
        counterP = counterP+1;
        for radius = 0 : 1 : 10
            x = radius*cos((angle*pi)/180)+newCoorMC(indexMC, 1);
            y = radius*sin((angle*pi)/180)+newCoorMC(indexMC, 2);
            activityTH = sqrt(sum((coorTH-ones(numTH, 1)*[x y]).^2,
2))*(((-1)*FmaxTH)/rfrTH)+FmaxTH;
            activityTH = activityTH.*(activityTH > 0);
            activityPattern(counterP, :) =
activityPattern(counterP, :)+(activityTH)';

            x = radius*cos(((angle+180)*pi)/180)+newCoorMC(indexMC, 1);
            y = radius*sin(((angle+180)*pi)/180)+newCoorMC(indexMC, 2);
            activityTH = sqrt(sum((coorTH-ones(numTH, 1)*[x y]).^2,
2))*(((-1)*FmaxTH)/rfrTH)+FmaxTH;
            activityTH = activityTH.*(activityTH > 0);
            activityPattern(counterP, :) =
activityPattern(counterP, :)+(activityTH)';
        end
    end

    FMCFinal = zeros(numMC, counterP);
    Vd = zeros(numMC, counterP);
    for iP = 1 : 1 : counterP
        Gexd = zeros(numMC, 2);
        Ginhp = zeros(numMC, 2);
        Ginhd = zeros(numMC, 2);
        FMC = zeros(numMC, 2);
        inputTH = (((activityPattern(iP, :)*Wth_mc)')*force)*Cth;
        for i = 1 : 1 : numTimeStep
            Gexd(:, 2) = (1-(1/Tau))*Gexd(:, 1)+(1/Tau)*(inputTH(:,
i)+Cexd*(setExd*FMC(:, 1)));
            Ginhp(:, 2) = (1-(1/Tau))*Ginhp(:,
1)+(1/Tau)*(Cinhp*(setInhp*FMC(:, 1)));
            Ginhd(:, 2) = (1-(1/Tau))*Ginhd(:,
1)+(1/Tau)*(Cinhd*(setInhd*FMC(:, 1)));
            Vp = (Gl*Gexd(:, 1))./((Gexd(:, 1)+Ginhd(:, 1)+1).*(Ginhp(:,
1)+Gl+1)+Gl*(Ginhp(:, 1)+1));
            if (i == numTimeStep)
                Vd(:, iP) = (Gexd(:, 1).*(Ginhp(:, 1)+Gl+1))./((Gexd(:,
1)+Ginhd(:, 1)+1).*(Ginhp(:, 1)+Gl+1)+Gl*(Ginhp(:, 1)+1));
            end
```

```
            FMC(:, 2) = (Vp.^3)./(0.01+(Vp.^3));
            Gexd(:, 1) = Gexd(:, 2);
            Ginhp(:, 1) = Ginhp(:, 2);
            Ginhd(:, 1) = Ginhd(:, 2);
            FMC(:, 1) = FMC(:, 2);
        end
        FMCFinal(:, iP) = FMC(:, 2);
    end

    data(indexMC, :) = FMCFinal(indexMC, :);

end

radius = 0.5/sin((60/180)*pi);
angle = 30 : 60 : 330;
coor = zeros(6, 2);
coor(:, 1) = radius*cos((angle*pi)/180);
coor(:, 2) = radius*sin((angle*pi)/180);

figure;
axis equal;
xlim([-5 5]);
ylim([-5 5]);
hold on;
angle = 0 : 1 : 179;
angle = (angle/179)*0.8-0.4;
for i = 1 : 1 : numMC
    x = coor(:, 1)+coorMC(i, 1);
    y = coor(:, 2)+coorMC(i, 2);
    fill(x, y, 'w');
    plot([coorMC(i, 1)-0.4 coorMC(i, 1)+0.4], [coorMC(i, 2)-0.25 coorMC(i,
2)-0.25], 'k', 'LineWidth', 2);
    tempX = angle+coorMC(i, 1);
    tempY = FMCFinal(i, :)*0.5+coorMC(i, 2)-0.25;
    temp = coorMC(i, 2)-0.25;
    for j = 1 : 1 : 180
        plot([tempX(1, j) tempX(1, j)], [tempY(1, j) temp], 'r');
    end
end

figure;
axis equal;
xlim([-5 5]);
ylim([-5 5]);
hold on;
for i = 1 : 1 : numMC
    x = coor(:, 1)+coorMC(i, 1);
    y = coor(:, 2)+coorMC(i, 2);
    fill(x, y, 'w');
end
for i = 1 : 1 : numMC
    for angle = 0 : 1 : 179
        radius = FMCFinal(i, angle+1)*0.6;
        x1 = radius*cos((angle*pi)/180)+coorMC(i, 1);
        y1 = radius*sin((angle*pi)/180)+coorMC(i, 2);
        x2 = radius*cos(((angle+180)*pi)/180)+coorMC(i, 1);
```

```
        y2 = radius*sin(((angle+180)*pi)/180)+coorMC(i, 2);
        plot([x1 x2], [y1 y2]);
        plot(coorMC(i, 1), coorMC(i, 2), 'r+');
    end
end

rand('twister', 5489);

counterP = 20;
num = 100;

corrYMC = zeros(num, 1);

Y = zeros(counterP, 1);
Y(counterP/2+1 : counterP, 1) = ones(counterP/2, 1);

for numUpdates = 1 : 1 : num

    FTH = rand(counterP, numTH);
    FTH(counterP/2, :) = ones(1, numTH)*((counterP/2)*0.5)-sum(FTH(1 :
counterP/2-1, :), 1);
    FTH(counterP, :) = ones(1, numTH)*((counterP/2)*0.5)-
sum(FTH(counterP/2+1 : counterP-1, :), 1);
    for i = 1 : 1 : numTH
        if (FTH(counterP/2, i) < 0)
            scaleFactor = ((counterP/2)*0.5)/sum(FTH(1 : counterP/2-1, i));
            FTH(1 : counterP/2-1, i) = FTH(1 : counterP/2-1,
i)*scaleFactor;
            FTH(counterP/2, i) = 0;
        elseif (FTH(counterP/2, i) > 1)
            scaleFactor = ((counterP/2)*0.5-1)/sum(FTH(1 : counterP/2-1,
i));
            FTH(1 : counterP/2-1, i) = FTH(1 : counterP/2-1,
i)*scaleFactor;
            FTH(counterP/2, i) = 1;
        end
        if (FTH(counterP, i) < 0)
            scaleFactor = ((counterP/2)*0.5)/sum(FTH(counterP/2+1 :
counterP-1, i));
            FTH(counterP/2+1 : counterP-1, i) = FTH(counterP/2+1 :
counterP-1, i)*scaleFactor;
            FTH(counterP, i) = 0;
        elseif (FTH(counterP, i) > 1)
            scaleFactor = ((counterP/2)*0.5-1)/sum(FTH(counterP/2+1 :
counterP-1, i));
            FTH(counterP/2+1 : counterP-1, i) = FTH(counterP/2+1 :
counterP-1, i)*scaleFactor;
            FTH(counterP, i) = 1;
        end
    end

    FMCFinal = zeros(numMC, counterP);
    Vd = zeros(numMC, counterP);
    for iP = 1 : 1 : counterP
        Gexd = zeros(numMC, 2);
```

```
        Ginhp = zeros(numMC, 2);
        Ginhd = zeros(numMC, 2);
        FMC = zeros(numMC, 2);
        inputTH = (((FTH(iP, :)*Wth_mc)')*force)*Cth;
        for i = 1 : 1 : numTimeStep
            Gexd(:, 2) = (1-(1/Tau))*Gexd(:, 1)+(1/Tau)*(inputTH(:,
i)+Cexd*(setExd*FMC(:, 1)));
            Ginhp(:, 2) = (1-(1/Tau))*Ginhp(:,
1)+(1/Tau)*(Cinhp*(setInhp*FMC(:, 1)));
            Ginhd(:, 2) = (1-(1/Tau))*Ginhd(:,
1)+(1/Tau)*(Cinhd*(setInhd*FMC(:, 1)));
            Vp = (Gl*Gexd(:, 1))./((Gexd(:, 1)+Ginhd(:, 1)+1).*(Ginhp(:,
1)+Gl+1)+Gl*(Ginhp(:, 1)+1));
            if (i == numTimeStep)
                Vd(:, iP) = (Gexd(:, 1).*(Ginhp(:, 1)+Gl+1))./((Gexd(:,
1)+Ginhd(:, 1)+1).*(Ginhp(:, 1)+Gl+1)+Gl*(Ginhp(:, 1)+1));
            end
            FMC(:, 2) = (Vp.^3)./(0.01+(Vp.^3));
            Gexd(:, 1) = Gexd(:, 2);
            Ginhp(:, 1) = Ginhp(:, 2);
            Ginhd(:, 1) = Ginhd(:, 2);
            FMC(:, 1) = FMC(:, 2);
        end
        FMCFinal(:, iP) = FMC(:, 2);
    end

    temp = zeros(numMC, 1);
    for i = 1 : 1 : numMC
        if (isequal(FMCFinal(i, :), zeros(1, counterP)) == 0)
            temp(i, 1) = corr(FMCFinal(i, :)', Y);
        else
            temp(i, 1) = 0;
        end
    end
    corrYMC(numUpdates, 1) = corr(Y, (FMCFinal')*temp);

end

display(num2str(mean(corrYMC.^2), '%4.3f'));
```

REFERENCES

ABELES M, GOLDSTEIN MH JR, FUNCTIONAL ARCHITECTURE IN CAT PRIMARY AUDITORY CORTEX: COLUMNAR ORGANIZATION AND ORGANIZATION ACCORDING TO DEPTH, J NEUROPHYSIOL. 1970 JAN;33(1):172-87.

ALBUS K, A QUANTITATIVE STUDY OF THE PROJECTION AREA OF THE CENTRAL AND THE PARACENTRAL VISUAL FIELD IN AREA 17 OF THE CAT. I. THE PRECISION OF THE TOPOGRAPHY, EXP BRAIN RES. 1975 DEC 22;24(2):159-79.

ALBUS K, A QUANTITATIVE STUDY OF THE PROJECTION AREA OF THE CENTRAL AND THE PARACENTRAL VISUAL FIELD IN AREA 17 OF THE CAT. II. THE SPATIAL ORGANIZATION OF THE ORIENTATION DOMAIN, EXP BRAIN RES. 1975 DEC 22;24(2):181-202.

BANKMAN IN, HSIAO SS, JOHNSON KO, NEURAL IMAGE TRANSFORMATION IN THE SOMATOSENSORY SYSTEM OF THE MONKEY: COMPARISON OF NEUROPHYSIOLOGICAL OBSERVATIONS WITH RESPONSES IN A NEURAL NETWORK MODEL, COLD SPRING HARB SYMP QUANT BIOL. 1990;55:611-20.

BENSMAIA SJ, DENCHEV PV, DAMMANN JF 3RD, CRAIG JC, HSIAO SS, THE REPRESENTATION OF STIMULUS ORIENTATION IN THE EARLY STAGES OF SOMATOSENSORY PROCESSING, J NEUROSCI. 2008 JAN 16;28(3):776-86.

CASANOVA MF (2005) NEOCORTICAL MODULARITY AND THE CELL MINICOLUMN, NOVA.

CREUTZFELDT O, INNOCENTI GM, BROOKS D, VERTICAL ORGANIZATION IN THE VISUAL CORTEX (AREA 17) IN THE CAT, EXP BRAIN RES. 1974;21(3):315-36.

ECCLES JC, THE PHYSIOLOGY OF NERVE CELLS, BALTIMORE: JOHNS HOPKINS, 1957.

FAVOROV OV, DIAMOND ME, WHITSEL BL, EVIDENCE FOR A MOSAIC REPRESENTATION OF THE BODY SURFACE IN AREA 3B OF THE SOMATIC CORTEX OF CAT, PROC NATL ACAD SCI U S A. 1987 SEP;84(18):6606-10.

FAVOROV O, WHITSEL BL, SPATIAL ORGANIZATION OF THE PERIPHERAL INPUT TO AREA 1 CELL COLUMNS. I. THE DETECTION OF 'SEGREGATES', BRAIN RES. 1988 JAN-MAR;472(1):25-42.

FAVOROV O, WHITSEL BL, SPATIAL ORGANIZATION OF THE PERIPHERAL INPUT TO AREA 1 CELL COLUMNS. II. THE FORELIMB REPRESENTATION ACHIEVED BY A MOSAIC OF SEGREGATES, BRAIN RES. 1988 JAN-MAR;472(1):43-56.

FAVOROV OV, DIAMOND ME, DEMONSTRATION OF DISCRETE PLACE-DEFINED COLUMNS--SEGREGATES--IN THE CAT SI, J COMP NEUROL. 1990 AUG 1;298(1):97-112.

FAVOROV OV, KELLY DG, MINICOLUMNAR ORGANIZATION WITHIN SOMATOSENSORY CORTICAL SEGREGATES: I. DEVELOPMENT OF AFFERENT CONNECTIONS, CEREB CORTEX. 1994 JUL-AUG;4(4):408-27.

FAVOROV OV, KELLY DG, MINICOLUMNAR ORGANIZATION WITHIN SOMATOSENSORY CORTICAL SEGREGATES: II. EMERGENT FUNCTIONAL PROPERTIES, CEREB CORTEX. 1994 JUL-AUG;4(4):428-42.

FAVOROV OV, KELLY DG, STIMULUS-RESPONSE DIVERSITY IN LOCAL NEURONAL POPULATIONS OF THE CEREBRAL CORTEX, NEUROREPORT. 1996 OCT 2;7(14):2293-301.

FOLDIAK P (1990) FORMING SPARSE REPRESENTATIONS BY LOCAL ANTI-HEBBIAN LEARNING. BIOL CYBERN 64: 165-170

FUJITA I, TANAKA K, ITO M, CHENG K, COLUMNS FOR VISUAL FEATURES OF OBJECTS IN MONKEY INFEROTEMPORAL CORTEX, NATURE. 1992 NOV 26;360(6402):343-6.

FYFE C (2005) HEBBIAN LEARNING AND NEGATIVE FEEDBACK NETWORKS. SPRINGER, LONDON.

GAWNE TJ, RICHMOND BJ, HOW INDEPENDENT ARE THE MESSAGES CARRIED BY ADJACENT INFERIOR TEMPORAL CORTICAL NEURONS? J NEUROSCI. 1993 JUL;13(7):2758-71.

GAWNE TJ, KJAER TW, HERTZ JA, RICHMOND BJ, ADJACENT VISUAL CORTICAL COMPLEX CELLS SHARE ABOUT 20% OF THEIR STIMULUS-RELATED INFORMATION, CEREB CORTEX. 1996 MAY-JUN;6(3):482-9.

GHOSE GM, OHZAWA I, FREEMAN RD, RECEPTIVE-FIELD MAPS OF CORRELATED DISCHARGE BETWEEN PAIRS OF NEURONS IN THE CAT'S VISUAL CORTEX, J NEUROPHYSIOL. 1994 JAN;71(1):330-46.

GOCHIN PM, MILLER EK, GROSS CG, GERSTEIN GL, FUNCTIONAL INTERACTIONS AMONG NEURONS IN INFERIOR TEMPORAL CORTEX OF THE AWAKE MACAQUE, EXP BRAIN RES. 1991;84(3):505-16.

HUBEL DH, WIESEL TN, RECEPTIVE FIELDS, BINOCULAR INTERACTION AND FUNCTIONAL ARCHITECTURE IN THE CAT'S VISUAL CORTEX, J PHYSIOL. 1962 JAN;160:106-54.

HUBEL DH, WIESEL TN, SEQUENCE REGULARITY AND GEOMETRY OF ORIENTATION COLUMNS IN THE MONKEY STRIATE CORTEX, J COMP NEUROL. 1974 DEC 1;158(3):267-93.

HUBEL DH, WIESEL TN, UNIFORMITY OF MONKEY STRIATE CORTEX: A PARALLEL RELATIONSHIP BETWEEN FIELD SIZE, SCATTER, AND MAGNIFICATION FACTOR, J COMP NEUROL. 1974 DEC 1;158(3):295-305.

IWAMURA Y, TANAKA M, SAKAMOTO M, HIKOSAKA O, DIVERSITY IN RECEPTIVE FIELD PROPERTIES OF VERTICAL NEURONAL ARRAYS IN THE CROWN OF THE POSTCENTRAL GYRUS OF THE CONSCIOUS MONKEY, EXP BRAIN RES. 1985;58(2):400-11.

JONES EG, HENDRY SHC, BASKET CELLS, CEREBRAL CORTEX VOLUME 1 CELLULAR COMPONENTS OF THE CEREBRAL CORTEX EDITED BY ALAN PETERS AND EDWARD G. JONES, 1984, 309-336.

MCKENNA TM, WHITSEL BL, DREYER DA, ANTERIOR PARIETAL CORTICAL TOPOGRAPHIC ORGANIZATION IN MACAQUE MONKEY: A REEVALUATION, J NEUROPHYSIOL. 1982 AUG;48(2):289-317.

MILLER KD, PINTO DJ, SIMONS DJ, PROCESSING IN LAYER 4 OF THE NEOCORTICAL CIRCUIT: NEW INSIGHTS FROM VISUAL AND SOMATOSENSORY CORTEX, CURR OPIN NEUROBIOL. 2001 AUG;11(4):488-97.

MOUNTCASTLE VB (1978) AN ORGANIZING PRINCIPLE FOR CEREBRAL FUNCTION: THE UNIT MODULE OF THE DISTRIBUTED SYSTEM. IN: THE MINDFUL BRAIN (MOUNTCASTLE VB, EDELMAN GM, EDS.), PP. 7-50. CAMBRIDGE, MA: MIT PRESS.

MOUNTCASTLE VB (1997) THE COLUMNAR ORGANIZATION OF THE NEOCORTEX. BRAIN 120: 701-722.

PETERS A, CHANDELIER CELLS, CEREBRAL CORTEX VOLUME 1 CELLULAR COMPONENTS OF THE CEREBRAL CORTEX EDITED BY ALAN PETERS AND EDWARD G. JONES, 1984, 361-380.

POWELL TP, MOUNTCASTLE VB, SOME ASPECTS OF THE FUNCTIONAL ORGANIZATION OF THE CORTEX OF THE POSTCENTRAL GYRUS OF THE MONKEY: A CORRELATION OF FINDINGS OBTAINED IN A SINGLE UNIT ANALYSIS WITH CYTOARCHITECTURE, BULL JOHNS HOPKINS HOSP. 1959

SEP;105:133-62.

RALL W, DISTINGUISHING THEORETICAL SYNAPTIC POTENTIALS COMPUTED FOR DIFFERENT SOMA-DENDRITIC DISTRIBUTIONS OF SYNAPTIC INPUT, J NEUROPHYSIOL. 1967 SEP;30(5):1138-68.

REICH DS, MECHLER F, VICTOR JD (2001) INDEPENDENT AND REDUNDANT INFORMATION IN NEARBY CORTICAL NEURONS. SCIENCE 294: 2566-2568

SCHÖLKOPF B, SMOLA AJ (2002) LEARNING WITH KERNELS. MIT PRESS, CAMBRIDGE

TOMMERDAHL M, FAVOROV O, WHITSEL BL, NAKHLE B, GONCHAR YA, MINICOLUMNAR ACTIVATION PATTERNS IN CAT AND MONKEY SI CORTEX, CEREB CORTEX. 1993 SEP-OCT;3(5):399-411.

TOMMERDAHL M., CHIU J, WHITSEL BL., AND FAVOROV O. (2005) MINICOLUMNAR PATTERNS IN THE GLOBAL CORTICAL RESPONSE TO SENSORY STIMULATION. IN: NEOCORTICAL MODULARITY AND THE CELL MINICOLUMN, MANUEL F. CASANOVA, M.D., ED., NOVA.

VAPNIK V (1995) THE NATURE OF STATISTICAL LEARNING THEORY. SPRINGER VERLAG, NEW YORK

VINJE WE, GALLANT JL, SPARSE CODING AND DECORRELATION IN PRIMARY VISUAL CORTEX DURING NATURAL VISION, SCIENCE. 2000 FEB 18;287(5456):1273-6.

ZOHARY E, SHADLEN MN, NEWSOME WT, CORRELATED NEURONAL DISCHARGE RATE AND ITS IMPLICATIONS FOR PSYCHOPHYSICAL PERFORMANCE, NATURE. 1994 JUL 14;370(6485):140-3. ERRATUM IN: NATURE 1994 SEP 22;371(6495):358.